Materials Today Electronics 6 (2023) 100058

Contents lists available at ScienceDirect

Materials Today Electronics

journal homepage: www.elsevier.com/locate/mtelec

Review

Formulation of functional materials for inkjet printing: A pathway towards fully 3D printed electronics

Anil Bastola [♯], Yinfeng He [♯,†], Jisun Im, Geoffrey Rivers, Feiran Wang, Robyn Worsley, Jonathan S. Austin, Oliver Nelson-Dummett, Ricky D. Wildman [*], Richard Hague [*], Christopher J. Tuck [*], Lyudmila Turyanska [*]

Centre for Additive Manufacturing, Faculty of Engineering, University of Nottingham, Nottingham NG7 2RD, United Kingdom

ARTICLE INFO

Keywords:
Ink formulation
Inkjet printing
Functional materials
Nanomaterials
Polymers
3D electronics

ABSTRACT

Inkjet printing offers a facile route for manufacturing the next generation of electronic devices, by combining the design freedom of additive manufacturing technologies with tuneable properties of functional materials and opportunities for their integration into heterostructures. However, to fully realise this potential, the library of functional materials available for additive manufacturing technologies needs to be expanded. In this review, we summarise current developments in ink formulation strategies, approaches for tailoring the functional properties of inks, and multi-material processing. Material – process – property relationships are reviewed for emerging functional materials, such as polymers, nanomaterials, and composites, with examples of current state-of-the-art devices. The flexibility of combining inkjet deposition with other existing technologies and a variety of substrates is also discussed reviewing current trends in electronics and optoelectronics, including wearable electronics, sensing, and energy applications. The review offers a comprehensive and systematic overview of ink formulations for inkjet deposition of electronic devices, summarising the challenges and perspectives in the advancement of 3D and multi-functional electronic devices and smart electronics.

1. Introduction

Additive manufacturing (AM), also known as three-dimensional (3D) printing, is a digital manufacturing process where objects are created in a layer-by-layer fashion directly from computer-aided-design (CAD) models. AM has emerged as a disruptive manufacturing process capable of creating highly intricate geometric designs with reduced material waste compared to traditional manufacturing processes [1–3]. Owing to its versatility and cost-effectiveness, AM has been used not only in rapid prototyping but also in large-scale applications to produce structural end-use parts in various fields, including but not limited to automobile, aerospace and civil engineering [4,5]. More recently, the focus of the research has moved to AM of functional materials relevant for applications in areas ranging from biomedicine [6,7] to electronics [8–10]. Structural AM typically focuses on creating customised and complex parts (e.g., lattice incorporated structures) to enhance the structural properties such as strength and weight, while the functional AM targets on creating parts to perform specific task or functions for examples conduct electricity, heat, magnetic field, etc.

AM of electronics is one example of functional AM and a rapidly growing field as it offers opportunities for the fabrication of low-cost, lightweight, intricate patterns [8,11]. Compared with conventional electronic manufacturing processes such as photolithography [12], plating [13] and vacuum deposition [14], AM of electronics can simplify the device processing by employing direct printing of materials with tailored properties into customized shapes and sizes. amongst a wide range of AM techniques, inkjet printing is considered the most promising approach for the deposition of functional materials for electronics, with potential of manufacturing multi-material structures [15,16]. Major advantages of the inkjet printing technique are its inherent compatibility

* Corresponding authors.
E-mail addresses: ricky.wildman@nottingham.ac.uk (R.D. Wildman), richard.hague@nottingham.ac.uk (R. Hague), christopher.tuck@nottingham.ac.uk (C.J. Tuck), lyudmila.turyanska@nottingham.ac.uk (L. Turyanska).
♯ Authors contributed equally.
† Current address: Nottingham Ningbo China Beacons of Excellence Research and Innovation Institute, University of Nottingham Ningbo China, Ningbo 315100, China.

https://doi.org/10.1016/j.mtelec.2023.100058
Received 29 June 2023; Received in revised form 25 August 2023; Accepted 8 September 2023
Available online 14 September 2023

with almost any substrate of interest, stemming from the additive, non-contact nature of the method, and its versatility to enable the manufacturing of complex structures. This offers the potential to produce lightweight, flexible, and foldable structures required for the next generation of smart electronics, wearable electronics, biomonitoring systems, medical devices, robotic e-skins, and others [17,18]. In inkjet printing, the structures are created by depositing droplets of ink through an array of micron-sized nozzles [19,20]. Large-area deposition can be achieved with high throughput rates by employing multiple nozzles [21]. The possibility to use highly tailored inks for electronics such as conductive polymer inks, for example, poly(3,4-ethylene dioxythiophene) polystyrene sulfonate (PEDOT:PSS) [22], polypyrrole (PPy) [23], polyaniline (PANI) [24], and poly-3-hexylthiophene (P3HT) [25] and nanomaterials such as graphene [26], carbon nanotubes (CNTs) [27], silver (Ag) [27], gold (Au) [28] and copper (Cu) [29], makes inkjet printing one of the best choices for manufacturing of printed electronic devices.

In recent years, there have been significant achievements in the field of printed electronics through the synergistic utilization of inkjet printing and high-performance materials [15,30]. Conductive materials are the basis for the manufacture of electronic devices and circuits and, as such, conductive inks were amongst the first to be developed for printed electronic applications – though largely for two-dimensional electronics. Therefore, there exists a large body of recent work on the deposition of conductive tracks via inkjet printing and their advancements, such as the optimisation of conductivity and expansion of substrate compatibility. Despite growing interest from industry and an increasing body of research, there remains a limited number of commercial inkjet printable functional materials available and thus a step-change in the understanding of the printing process / material properties relationship is needed to truly unleash the potential of AM for 3D electronics.

The current approach to printing electronic devices and multi-material heterostructures requires changing the ink cartridge and/or the substrate during the printing process [31–33]. This allows for the creation of multi-material planar structures in 2D, and for extending them into 3D heterostructures [31]. However, this approach is unable to control ink deposition in a voxel manner, which is necessary for creating functional 3D electronic devices without further steps such as assembly or post-processing. Manufacturing of 3D integrated functional electronics such as circuit boards, where the components such as wiring, power source, and packaging are all fabricated by a single process is required. It should be noted that inkjet printing is a forefront technique because its drop-on-demand (DOD) and high-resolution motifs enable voxel-based multi-material printing for fully 3D printed integrated electronics. Inkjet printing is a promising method for both 2D planar and integrated 3D electronic devices. Integrated 3D printed electronic devices can be created by combining 2D planar devices, often as heterostructures. To enable fully 3D printed electronics, where complex 3D structures can be directly printed from CAD data, advancemnts in multimaterial AM technologies and availability of functional material formulations need to be achieved.

The primary considerations to achieve fully 3D printed integrated electronic include: ensuring that the raw functional material is well dispersed and loaded in the ink solution to achieve good jettability/printability; understanding and optimizing the electronic performance of the deposited material and interfaces; and efficient post-processing such as sintering and curing. Therefore, a comprehensive understanding of these factors is crucial, whether in developing heterostructures or planar structures, as well as a voxel-based multi-material inkjet printing (MM-IJ3DP). While MM-IJ3DP offers the possibility to realise complete 3D integrated electronics by accounting for the aforementioned factors just in a single process, yet the ink components and formulation remain key. Current reviews typically focus on a specific group of materials [34,35] or on a specific application [36,37]. However to enable sugnificant advancement of AM of electronics, dielectric, semiconducting and metallic material is needed. This can be enabled by comprehensive understanding of the approaches to the ink formulations, underpinning expansion of AM compatible materials, and by systematic review of the interconnectivity between the formulation and function in the AM process.

This review transcends the above-mentioned fields, providing a summary of the ink formulating strategy for inkjet deposition of functional materials, manufacturing strategy for co-printing of multiple materials and specific functions achieved. We discuss a range of materials for 3D electronic devices (polymers, nanomaterials and composites), their functionalities that can be achieved through inkjet deposition, and challenges associated with the performance of inkjet deposited multi-material structures. These concepts are illustrated with examples of state-of-the-art devices, from sensors and detectors to 3D electronics (Fig. 1). The review focuses on advancements made and remaining challenges of inkjet of electronic devices, including sensors, energy storage, and fully-3D-printed integrated electronics.

2. Functional material inks for inkjet printing

Functional material inks suitable for inkjet manufacturing of electronics are increasingly expanding with the evolution of new ink formulations and advancement in printhead technologies, where several inks and printheads are now commercially available. The strategies successfully used for polymeric, nanomaterial, and composite ink materials for inkjet printing are discussed here. To formulate the inks, a number of parameters need to be accounted for, such as ink rheology, which defines the jetting and jetting stability, as well as contact angle and coffee ring effects, that control the resolution, surface finish and uniformity of the printed structure.

2.1. Ink formulation strategy

The ink consists of various materials such as solvent, particles, and surfactants. The stability and jettability of the ink, print resolution, and uniformity of jetted layers are key factors in formulating suitable inks for inkjet printing [19]. During the inkjet printing process, the ink undergoes three different stages: ejection, deposition/spreading, and drying, which all require careful consideration of the ink's raw materials to minimize side effect that cause either printer failure or poor print quality.

The key requirements for DOD-based ink formulations include stability against aggregation and precipitation, and stability in jetting. The printing stability is governed by the physical properties of the ink, where a Z-value is normally used as an indicator for the jettability of the ink. Z-value is a dimensionless inverse of the Ohnesorge (Oh) number:

$$Oh = 1/Z = \frac{\sqrt{We}}{Re} = \frac{\eta}{\sqrt{\gamma \rho a}} \quad (1)$$

where $Re = v\rho a/\eta$ is the Reynolds number, $We = v^2\rho a/\gamma$ is the Weber number, ρ is the density, η is the dynamic viscosity, γ is the surface tension, v is the velocity of the fluid, and a is nozzle diameter [38]. The jettable zone is highlighted in the Fig. 2a. A Z-value between 1 and 10 is normally considered suitable for inkjet printing.

The ink composition also affects jetting, where inks with solid or gel particles are preferred; to prevent nozzle clogging, a commonly used criterion is that the solid or gel particle size should be below 1/50th of the nozzle diameter [20]. The strategy includes the identification of suitable solvents [41], surfactants [42], and binders [43]. For nanomaterials with poor dispersibility, surface functionalisation with organic materials is used to help improve dispersibility and stability. However, a post-processing step is often required as the presence of organic materials can influence the electrical properties of these layers [44]. The ink viscosity, surface tension and density are optimised to achieve stable droplet formation using surfactants, polymers, and solvents. For

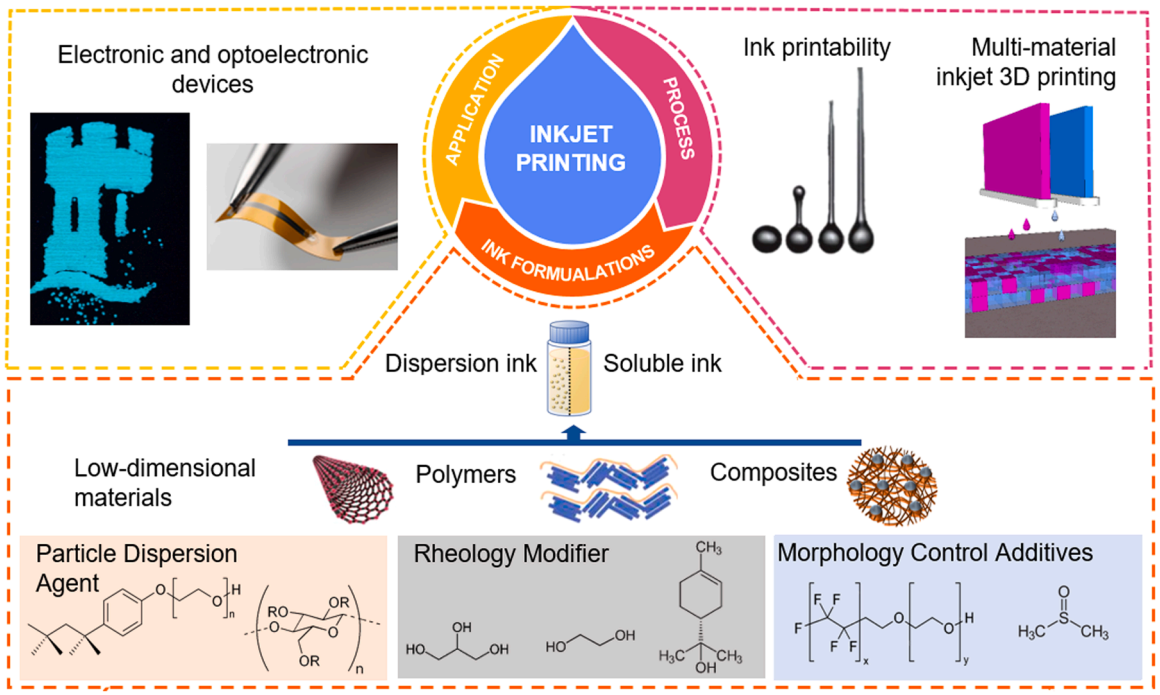

Fig. 1. Schematic representation of inkjet printing, from ink development and materials, used, and deposition and post-deposition process to examples of applications.

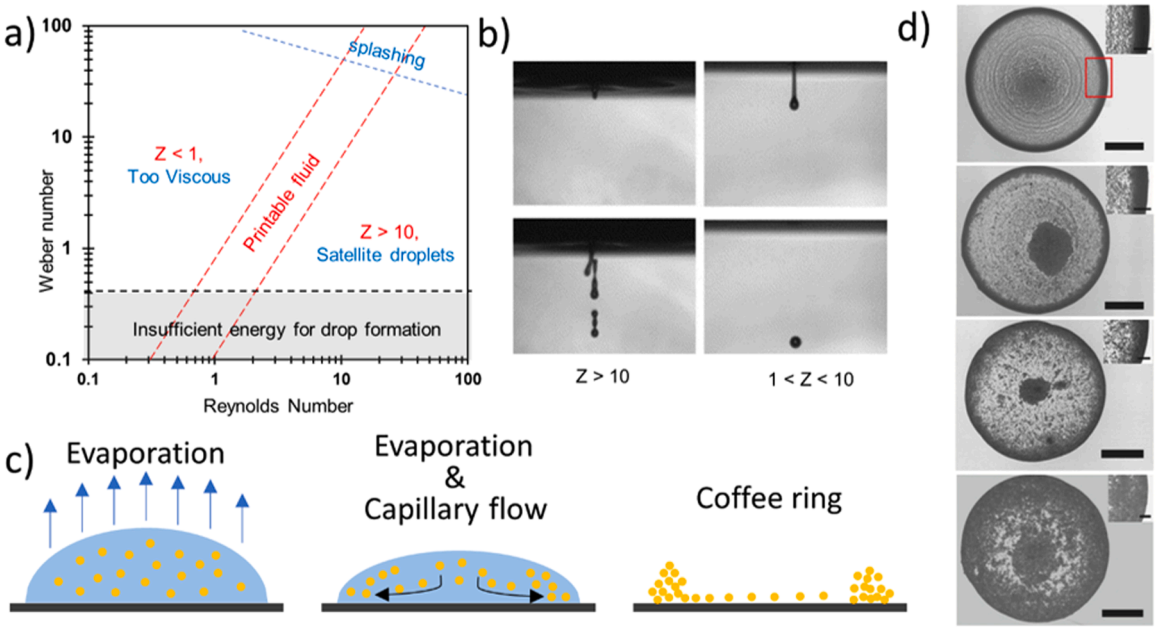

Fig. 2. Ink droplet formation and deposition. a) The inkjet printable regime is shown in the plot between the Weber number and Reynolds number (adapted from Ref. [21]). **b)** Discharge images of inks illustrating the effect of the value of Z (reproduced from Ref. [39]). **c)** Schematic of the drying process and coffee ring effect. **d)** SEM images of printed GO ink droplets on Si/SiO_2 substrates after drying at 30 °C showing a transition from a clear coffee ring to a uniformly dried deposit due to the Marangoni effect as the flake size increases from 500 nm (top image) to 5 mm (bottom image) (reproduced from Ref. [40]). Scale bars are 100 μm in the main images and 20 μm in the insets.

example, polystyrene [45], ethylene glycol, propylene glycol, and glycerol [46] have also been effective in enhancing the viscosity in many ink formulations [31,47,48].

The droplet deposition and print resolution are governed by ink spreading and drying. For drops deposited at a separation distance, *s*, the print resolution on the substrate can be calculated as $R = \frac{2{,}540.0}{d+s}$, where *d* is the droplet diameter. Several techniques can be applied to enhance wettability, including the modification of ink formulations [49,50], substrate coating and surface plasma treatment with oxygen, ultraviolet (UV), and ozone (O_3) [50,51]. The addition of surfactants, for example, surfynol [52] and didodecyldiphenyl ether disulfonate [53] is considered to lower the surface energy of the ink and has also been reported to enhance the ink wetting and pinning. However, the increased wetting can reduce manufacturing resolution, hence optimization of the ink

formulation is focused on ensuring the balance between the pinning and the feature size.

The uniformity of printed structures [54] can be affected by phenomena such as the coffee ring effect and Marangoni flow [40] (Fig. 2c). The coffee ring effect is induced as a result of a combination of contact line pinning and capillary flow [55], and determine the morphology of the final print. To prevent the coffee ring effect, evaporation should be driven by flow due to surface tension gradients, known as Marangoni flow [55,56], instead of capillary flow. Marangoni flow can be induced by increasing the substrate temperature [57,58], use of high boiling point co-solvents (e.g., diethylene glycol (DEG) and formamide (FA)) with a low boiling point main solvent (e.g., water) [59,60]), and by improving the thermal conductivity between the printed droplet and the substrate [61]. Hence, to achieve high printing resolution and uniformity, deposition of a solute or ink needs to be optimised by controlling wettability and Marangoni flow for reproducible production of high-performance printed electronics [56,62]. To eliminate the coffee ring effect, Matavz et al. [46] developed Ta-Al-Si-alkoxide-based dielectric ink formulations with 2-methoxyethanol as the main solvent and highly viscous glycerol or 1,3-propanol as the co-solvent for optimal viscosity and surface tension. However, a pronounced "coffee-ring" effect was observed due to the higher volatility of 2-methoxyethanol compared to the viscous solvents. Consequently, the recirculating Marangoni solvent flow exists only at the onset of drying and ceases to exist once the 2-methoxyethanol has completely evaporated from the drying feature. The combination of all three solvents appears to prolong the duration of the Marangoni flow, resulting in improved uniformity of dried structures and better device performance. Hu et al. [63] investigated isopropanol (IPA)-based alcohol mixtures in various 2D crystal inks including graphene, hexagonal boron nitride (h-BN), bismuth telluride (Bi_2Te_3), indium selenide (In_2Se_3), and black phosphorus (BP). IPA is widely used as a solvent for graphene inks and, recently, for 2D crystal inks due to its support for a metastable dispersion of the 2D crystal nanoflakes and its low surface tension for good wetting on

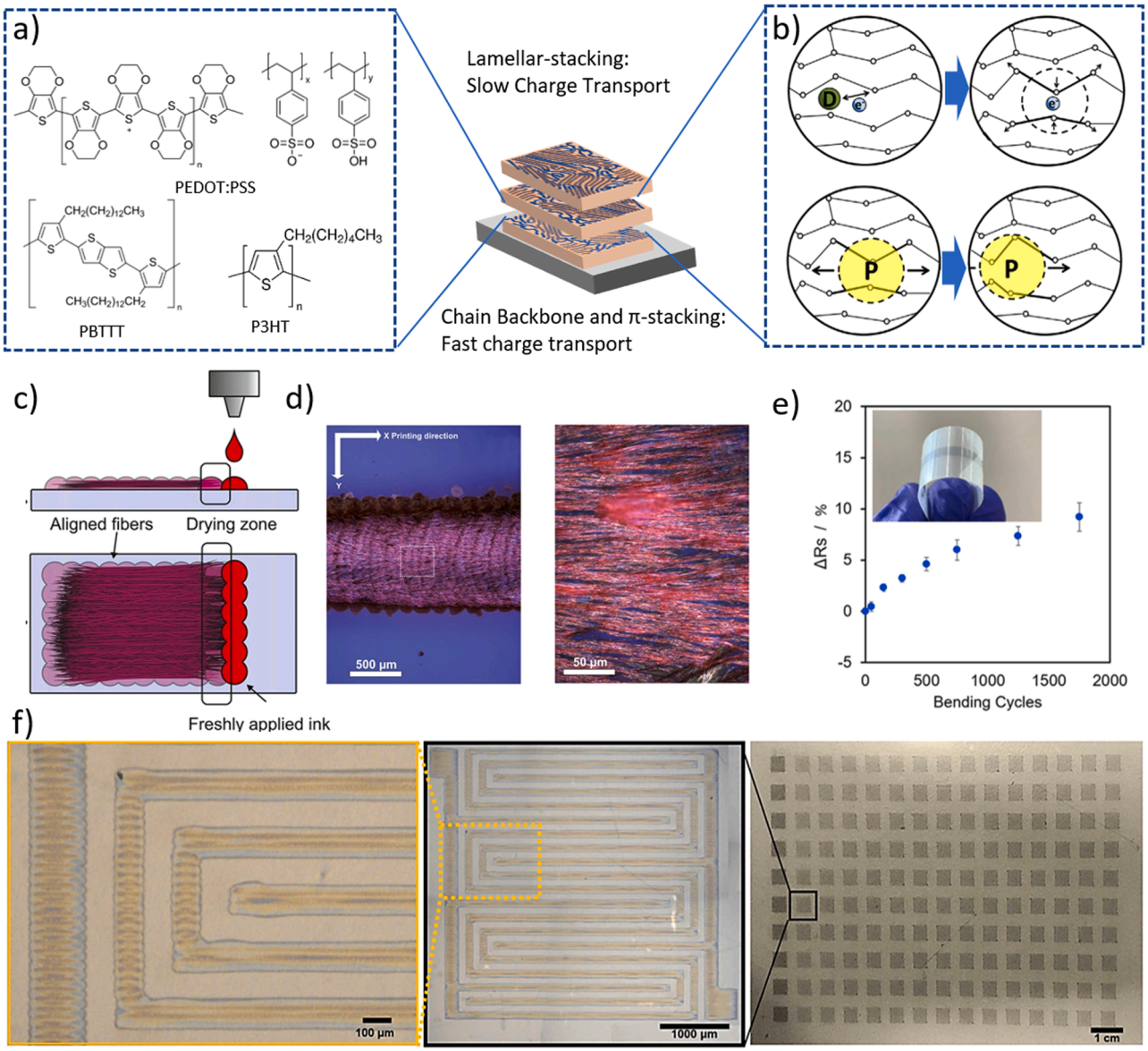

Fig. 3. Overview of inkjet printed conductive polymers. **a)** Examples of commonly used conductive polymers. **b)** Summary of charge transfer rates with respect to chain backbone orientation. (Reproduced from Ref. [72] **c)** Schematic illustration of aligned p3HT fibres forming based on printing-induced shear-directed crystallization. **d)** Optical image of the orientated p3HT fibres in the printed line ((c-d) reproduced from Ref. [74]). **e)** Relative resistance of ink jetted PEDOT:PSS flexible substrate undergoing bending and **f)** An example of stable large area PEDOT:PSS ink jetting, 140 serpentine electrodes measuring 10 cm x 6.3 cm without defects such as bulged lines, missing swaths, missing droplets, or misplaced droplets (e-f reproduced from Ref. [22]).

substrates [63,64]. However, the coffee ring effect persists with IPA-based 2D crystal inks. Hu et al. [63] studied the drying mechanism of a binary solvent ink formulation, where Marangoni-enhanced spreading inhibits contact line pinning and deforms the droplet shape to naturally suppress the capillary flow that gives rise to the coffee ring effect. Liu et al. [65] also demonstrated a binder-free ink composed of black phosphorous and a binary solvent mixture of isopropanol and 2-butanol. He et al. [40] suggested that different particle size can also influence the coffee ring effect where smaller particles (500 nm) shows less significant coffee ring than the large ones (5 μm) (Fig. 2d). The ink formulation allows stable jetting, induces recirculating Marangoni flow to control the coffee ring effect, and ensures wetting of untreated substrates.

2.2. Polymeric inks

Polymers are of high value in printed electronics, due to their highly variable and tailorable properties, including flexibility [66], biocompatibility [67], electrochemical activity, [68] electrical properties [69], etc. To deposit polymeric materials, inks are formulated using monomers/copolymers, which are usually polymerised in the AM process or in a secondary step.

2.2.1. Conductive polymeric inks

To date, a number of conjugated polymers is commonly used for inkjet deposition, including poly(3,4-ethylenedioxythiophene) polystyrene sulfonate (PEDOT:PSS), polypyrrole (PPy), polyaniline (PANI) and poly(3-hexylthiophene-2,5-diyl) (P3HT), and poly(2,5-bis(3-alkylthiophen-2-yl)thieno[3,2-*b*]-thiophene) (PBTTT) (Fig. 3a). amongst those, PEDOT:PSS has received significant attention due to its ability to form aqueous suspensions and high conductivity (up to 1418 S cm^{-1} [70]). The conductivity is dependant on radical charge transfer along with delocalized electron orbitals of the polymer backbone through hopping (Fig. 3a,b) and materials are oxidised or reduced to respectively achieve p-type [71] or n-type [72] conduction. The degree of doping and redox states provide avenues to improve conductivity [73] where charge transfer is dependant on the orientation of current flow relative to the conductive backbone of the polymer and any local crystalline order (Fig. 3b).

The formulation of conductive polymer inks remains challenging, due to a high degree of chain interaction, resulting in poor solubility and high viscosities [75]. The polymers with regularly spaced non-polar side chains or groups such as P3HT, PBTTT, polyvinylcarbazole (PVK), poly(N,N'-bis-4-butylphenyl-N,N'-bisphenyl)benzidine (Poly-TPD), or dodecylthiophene (PC12TV12T) can be fully dissolved in non-polar or chlorinated solvents for use as low-concentration inks (< 1.5 wt.% [76]). Poorly soluble polymers are either printed using dispersions of nanoparticles or gels stabilised by dopant complexes (< 1.5 wt.%, e.g., PEDOT:PSS, PANI, PPY), or are synthesised post-printing through the jetting of reactive precursor inks (e.g., PVK, PPy, and PANI). For multi-phase inks, co-solvents and surfactants are commonly used to improve their printability and wettability (e.g., gemini surfactants and ethanol in PPy nanodispersion were used to reduce surface tension to 30.8 mN m^{-1}, compared to 69.8 mN m^{-1} without optimisation [23]), while crosslinkers provide post-print stabilisation (e.g. (3-glycidyloxypropyl)trimethoxysilane (GOPS), divinyl sulfone (DVS), and diacetylene diol (DADOL) [25]).

In addition to the above modifications to fluid and film mechanics, some additives alter the electronic properties of the conductive polymers through chemical doping and microstructural ordering and are employed to influence the electrical properties of the polymers [77]. Additives, such as 1,3,5-trichlorobenzene (TCB) can promote ordering in PC12TV12T or polyTPD, [78], resulting in significant improvements in device performance. For example, P3HT crystalline nanofibers used in organic field-effect transistors (OFETs) improved 5-fold in drain current and 40-fold in on-off ratio compared to isotropic P3HT [74] (Fig. 3c). Due to the presence of an ionic bond between the conductive PEDOT and non-conductive PSS molecules, additives with a screening effect are used to achieve favourable microstructures and increase conductivity [71]. To date, dimethyl sulfoxide (DMSO) (1000 S cm^{-1} [79]), anionic surfactants (80 S cm^{-1} with the addition of sodium dodecyl sulfonate (SDS) [80], 542 S cm^{-1} with the addition of dodecylbenzene sulfonic acid (DBSA) were successfully used (Table 1). However, additives that alter interchain interactions can also increase viscosity or reduce ink stability,

Table 1
Summary of formulations, post-processing parameters and electrical properties of low dimensional materials and conductive polymers.

Material / solvent	Particle size, concentration	Processing, Post-processing	Sheet resistance (R_s), conductivity (σ) and mobility (μ)	Refs
0D inks				
Ag / ethylene glycol	5 - 50 nm	250 °C (curing)	$R_s = 10$ μΩ cm	[85]
Ag / water-ethylene glycol	< 30 nm	150 °C (curing)	$R_s = 12.6$ μΩ cm	[86]
Ag / triethylene glycol monoethyl ether	5 - 8 nm	–	$R_s = 12.6$ μΩ cm	[87]
Au / xylene	3 nm	180 °C (IR drier)	$R_s = 16$ μΩ cm	[88]
Au / petroleum hydrocarbon based non-aromatic solvent	2 –10 nm	200 °C	$R_s = 20$ μΩ cm	[89]
Cu / water-ethylene glycol	126 nm	Photonic sintering	$R_s = 40$ μΩ cm	[29]
Cu	–	Photonic sintering	$R_s = 5$ μΩ cm	[90]
Ni	3000 nm	Photonic sintering	$R_s = 50{,}000$ μΩ cm	[91]
1D and 2D inks				
SWCNT-COOH / water	24 μg/mL	–	$R_s = 2$ kΩ/sq for 14 layers	[92]
SWCNT / water	0.15 mg/mL	–	$R_s = 760$ Ω/sq for 12 prints	[42]
MWCNT / water	–	–	$R_s = 16$ kΩ/sq	[93]
Graphene / cyclohexanone and terpineol	3.5 mg/mL	950 °C (annealing)	$R_s = 172.7$ kΩ/sq	[94]
Graphene / DMF	2 mg/mL	400 °C (annealing)	$\sigma = 3400$ S/m	[95]
rGO / styrene - divinylbenzene - glycerol	0.5 mg/mL	Pre reduced	$R_s = 2.14$ kΩ/sq for 12 layers	[96]
hBN / water	2 mg/mL	150 °C (annealing)	Capacitance 2.0 ± 0.3 nF cm^{-2} for ~3 μm layer	[97]
Polymeric inks				
PEDOT:PSS / water	1.1 wt.%	Reactive ink-jetting	$\sigma \leq 800$ S cm^{-1}	[83]
PEDOT:PSS / water	1.1 wt.%	–	$\sigma = 360$ S cm^{-1}	[25]
	0.5–1 wt.%		$\sigma = 295 \pm 10$ S cm^{-1}	
P3HT / chlorobenzene	0.16 wt.%	–	$\mu \sim 0.002$ to 0.017 $cm^2 V^{-1} s^{-1}$	[74]
PBTTT / trichlorobenzene	0.5 wt.%		$\mu \sim 0.05$ to 0.1 $cm^2 V^{-1} s^{-1}$	[98]
PPy / water	0.3–0.89 M	Reactive ink-jetting	$R_s \sim 25$ kΩ/sq on textiles	[99]
PPy / water	various	–	$\sigma \leq 4.95$ S cm^{-1}	[23]
PANI / water	0.2–1.2 M	Reactive ink-jetting	$R_s \sim 1$ kΩ/sq on textiles	[99]

hence their concentration has to be optimised to enable jettability [81,82]. For this reason, ionic liquids were found unsuitable for single-mixture PEDOT:PSS inks (viscosity > 40 cP at 1 wt.% 1-ethyl-3--methylimidazolium ethyl sulphate (EMIM:ES), while reaching 900 S cm^{-1} with 2.0 wt.% EMIM:ES [83]), except at very low concentrations (less than 0.5 wt.% ionic liquids [84]) in which case the gelation effect and increased chain mobility also enhanced stretchability. To date, the highest achieved conductivity of an inkjet polymer is 1000 S cm^{-1} for PEDOT:PSS containing 5 wt.% DMSO and 464 S cm^{-1} for a layer-stablished PEDOT:PSS containing 1 wt.% GOPS [25].

After printing, both thermal annealing and chemical treatment are commonly used to control and modify the properties of printed layers. For PEDOT:PSS, significant enhancement of conductivity was achieved by immersion in dimethylformamide (DMF), ethylene glycol (EG), DMSO, or sulfuric acid (723 S cm^{-1}[100], 1418 S cm^{-1}[70], 1185 S cm^{-1} [101], and 4200 S cm^{-1} [102]). The effect of thermal annealing on electrical properties is also dependant on the additives present, with a small effect observed in pristine PEDOT:PSS (0.15 S cm^{-1} uncured, 0.3 S cm^{-1} 225 °C for 20 min), compared to the significant importance in glycerol-doped PEDOT:PSS (35 wt.% glycerol, < 1 S cm^{-1} uncured, 82.5 S cm^{-1} 150 °C for 20 min [103]). Recently (2023), highly reliable large-area printing of PEDOT: PSS which is stable under bending, annealing, and exposure to UV or IR light (using the bio-renewable solvents dihydrolevoglucosenone (cyrene) and glycerol carbonate (GC) as alternatives to DMSO) for flexible electronics was reported [22] (Fig. 3e,f).

Recently, micro-reactive inkjet deposition has been employed to bypass inkjet's limitations and achieve higher performance layers, wherein two low-viscosity precursor inks are combined to synthesize or modify the conductive polymer in-situ. This has been demonstrated for sequentially-reacted inkjet-printed PANI (0.11 S cm^{-1} [104], 1 kΩ sq^{-1} on textiles [99]), PPy (25 kΩ sq^{-1} on textiles [99]). Micro-reactive inkjet printing of PEDOT:PSS and ionic liquid additive EMIM:ES results in the development of a highly conductive PEDOT:PSS microstructure (>50 cP, 900 S cm^{-1} with 2.0 wt.% EMIM:ES, [83]).

2.2.2. Insulating and dielectric polymeric inks

Several ink-jettable dielectrics and insulating polymers have been demonstrated, including poly-4-vinylphenol (PVP) [105], tripropylene glycol diacrylate (TPGDA) [106], photoresist epoxy (brand name SU-8) [107], polysiloxane [108], and poly(amic) acid (PAA) (subsequently thermally reacted into polyimide) [109]. The presence of pinhole defects in inkjet dielectric layers is commonly detrimental to device performance [105]. One strategy is to jet photo- or thermally-initiated inks of reactive monomers or short reactive oligomers, such as TPGDA (with 2,4-diethyl-9h-thioxanthen-9-one (DETX) and ethyl 4-(dimethylamino) benzoate (EDAB) photoinitiator and synergist, respectively [106]) and diluted epoxides such as SU-8 [107] (reported with a high dielectric constant of 3, achieved for a 200-nm-thick layer of polysiloxane thermally crosslinked at 135 °C [108]). Recently, inkjet printing of polydimethylsiloxane (PDMS) elastomer inks at high concentrations was demonstrated for reactive-inkjet, with one ink containing silicone hydride, and second ink containing the silicone oligomer and a Pt catalyst (both with 60 wt.% in octyl acetate) [66]. Examples of 3D constructs were reported with individual reactive layers with a thickness of 12.1 μm [66].

A second strategy is based on solvent-diluted inks of polymers, such as commercial non-reactive PVP ink (dielectric constant of 3.9 [105]) or self-reacting poly(amic) acid (relative permittivity of 3.41 [109]). For control of layer thickness in heterostructures, optimisation of the polymer concentration, droplet spacing, and thermal treatment is effective: PVP with a thickness of ~70 nm was achieved by drying at 90 °C for 10 min followed by 130 °C for 20 min [105], while rapid drying of PAA/-polyimide ink at substrate temperatures of 120 °C, 150 °C, and 180 °C resulted in a dried layer thickness of 1.0 μm, 1.5 μm, and 2.0 μm, respectively [110] Further modifications of these inks are possible with additives that crosslink the polymer at available reactive sites (e.g. hydroxyl groups of PVP, crosslinked by (poly(melamine-co-formaldehyde) (PMF); 15 wt.% PVP, 5.8 wt.% PMF in ethanol [111]).

2.3. Nanomaterial-based inks

Nanomaterials, also referred to as low-dimensional materials, have great potential in a wide range of functional electronic devices due to their superior electrical, mechanical, thermal, optical, and optoelectronic properties. Low dimensional inks for electronics can be categorized as nanoparticle (0D) inks, which include for example AgNP, AuNP, CuNP inks [112], nanotube- and nanorod-based (1D) inks, such as CNT-based inks, and 2D nanomaterial inks, which include exfoliated layered material inks, such as graphene, hexagonal boron nitride (hBN), and transition metal oxides. We note that the dimensionality of the nanomaterials affects their physical and functional properties, as a result of quantum confinement effects, and the requirements for ink formulations are different for nanomaterials with different dimensionality. For example, 0D nanoparticles have a layer of capping ligands, that define their interaction with the solvent. This is not the case for e.g., 2D materials, hence different considerations need to be made to achieve jettable formulations.

2.3.1. Nanoparticle-based inks

Conductive inks based on metal nanoparticles (NPs) are one major category of printed conductive tracks. Dispersion of metal NPs makes it jettable through micron-sized nozzles which can be sintered at lower melting temperatures compared to their bulk counterparts due to their high surface area-to-volume ratio. They exhibit relatively low electrical resistivities (5–40 μΩ cm, Table 1). Synthesis and ink formulation strategies for ligand-functionalised NPs with narrow size distribution have been developed to ensure long-term ink stability and jetting quality of nanoparticulate conductive inks. To date, AgNP inks are the most common [113,114], however different metal NP including gold, copper and nickel are increasingly being investigated (Table 1). Common surface ligands for AgNP inks are poly(acrylic acid) (PAA) [115] and poly (vinylpyrrolidone) (PVP) [15,85]. These inks offer a low-temperature sintering process (< 150 °C), suitable for flexible substrate deposition (e.g., PET film), and good cohesion between droplets and improved adhesions to various substrates, including Si/SiO_2 wafers, glass, paper and polymer films [15,44]. However, anisotropic electrical conductivity, where vertical conductivity is lower than planar conductivity, is observed due to the presence of organic residues concentrated between vertically stacked printed layers [27,87,116].

AuNP ink is particularly advantageous for bioelectronics that is operational in harsh environments, such as high humidity and salt-rich fluids (e.g., body sweat) due to its chemical stability and biocompatibility [28]. Hydrophilic AuNPs protected by a sparse layer of ionic ligands were prepared for ink formulation by the introduction of a mixed ligand shell comprising an ω-functionalised ionic ligand and a labile ligand, with subsequent selective removal of the labile ligands. A sparse layer of ligands on AuNPs compared with conventional dense ligands enables destabilisation of the ligand shell at a lower sintering temperature (~150 °C) suitable for polymeric substrates without losing the critical surface ionic density for dispersibility and increased electrical conductivity [117]. Introduction of multifunctional thiol, trimethylolpropane tri(3-mercapto propionate), as a cohesion enhancer in the ink formulation of octane thiol-functionalised AuNPs improved the cohesion and integrity of AuNPs [118].

CuNP ink offers a cost-effective alternative to Au and Ag inks, however, the susceptibility of Cu to oxidation even before and/or during printing and sintering hinders its application. A precursor-type Cu ink provides a route to overcome Cu oxidation during ink storage, printing, and sintering. The ink containing hydrous copper formate with 2-amino-2-methyl-1-propanol (CuF-AMP) is chemically stable and has a low viscosity solution even with high loading, and sintering at 190 °C

provides reasonable electrical properties (10.5 μΩ cm) [119]. CuO dispersion ink consisting of water and ethylene glycol coupled with the pulse-thermal process is another route to eliminate particle oxidation [29].

Apart from metal NPs, colloidal semiconductor quantum dots (QDs) and perovskite nanocrystals (NCs) are also attracting significant attention due to their tuneable optical properties in a wide range of the electromagnetic spectrum, from visible to short-wave infrared [120]. QD inks developed in various solvents, including N-methyl-2--pyrrolidone (NMP) with 1 wt% of n-butylamine (BTA), provide stable formulations over several days and high-resolution printing of a thin uniform film [120]. Despite the significant potential, the perovskite stability in ambient conditions also remains to be addressed [121]. Recent research reports demonstrate the enhancement of optical stability of QDs and perovskite NCs in inkjet printed films, however further work is still needed.

2.3.2. 1D nanomaterials based inks

The field of inkjet printing with 1D material inks is still in its infancy, partially due to challenges with dispersion of 1D materials in inks, as well as controlling their organization in the printed layers [122,123]. Amongst 1D materials, carbon nanotubes (CNTs) provide the opportunity for mass-manufacturable, high-performance printed and flexible large-area electronics due to their impressive mechanical and electrical properties [36]. However, the strong tendency of CNTs to form large bundles due to strong van der Waals interactions (~500 eV um-1) and high aspect ratio (>1000) limits their dispersibility [124]. Noncovalent functionalisation of CNTs with polymers (i.e. polymer wrapping) [36] and various types of surfactants (e.g., naphthyl-group-based non-ionic surfactant) [42] has emerged as a very effective technique utilising van der Waals force and π-π interaction to achieve good dispersion for inkjet printing. Soum et al. [35] demonstrated an aqueous CNT ink consisting of multi-walled CNTs (MWCNTs) wrapped with naphthyl-functionalised poly(ethylene glycol) surfactants for a fingerprint sensor device (Fig. 4a-c).

Integration of 1D materials with different composition, such as metal nanomaterials, with inkjet printing was explored with Ag nanowires [122,128], Au nanorods [129] and semiconductor nanorods [130]. Conductive silver nanowires have also gained great interest due to their high electrical conductivity even at very low concentrations, compared to AgNP-based conductive inks, and high aspect ratio. However, nozzle clogging due to flow-induced nanowire alignment when passing through a nozzle presents challenges for jetting. Patil et al. reported optimal Ag nanowire length of 1.7 μm for smooth passage of nanowires through a nozzle [123]. Enhanced stability and conductivity can be also achieved by addition of a conductive polymer, polyaniline, as a stabilizing agent.

Of particular interest are the opportunities offered by anisotropic properties of 1D materials, which can enable ordering and alignment of these nanomaterials within the final structure, as was recently demonstrated for Au nanorods [131] and semiconductor CdSe/CdS nanorods

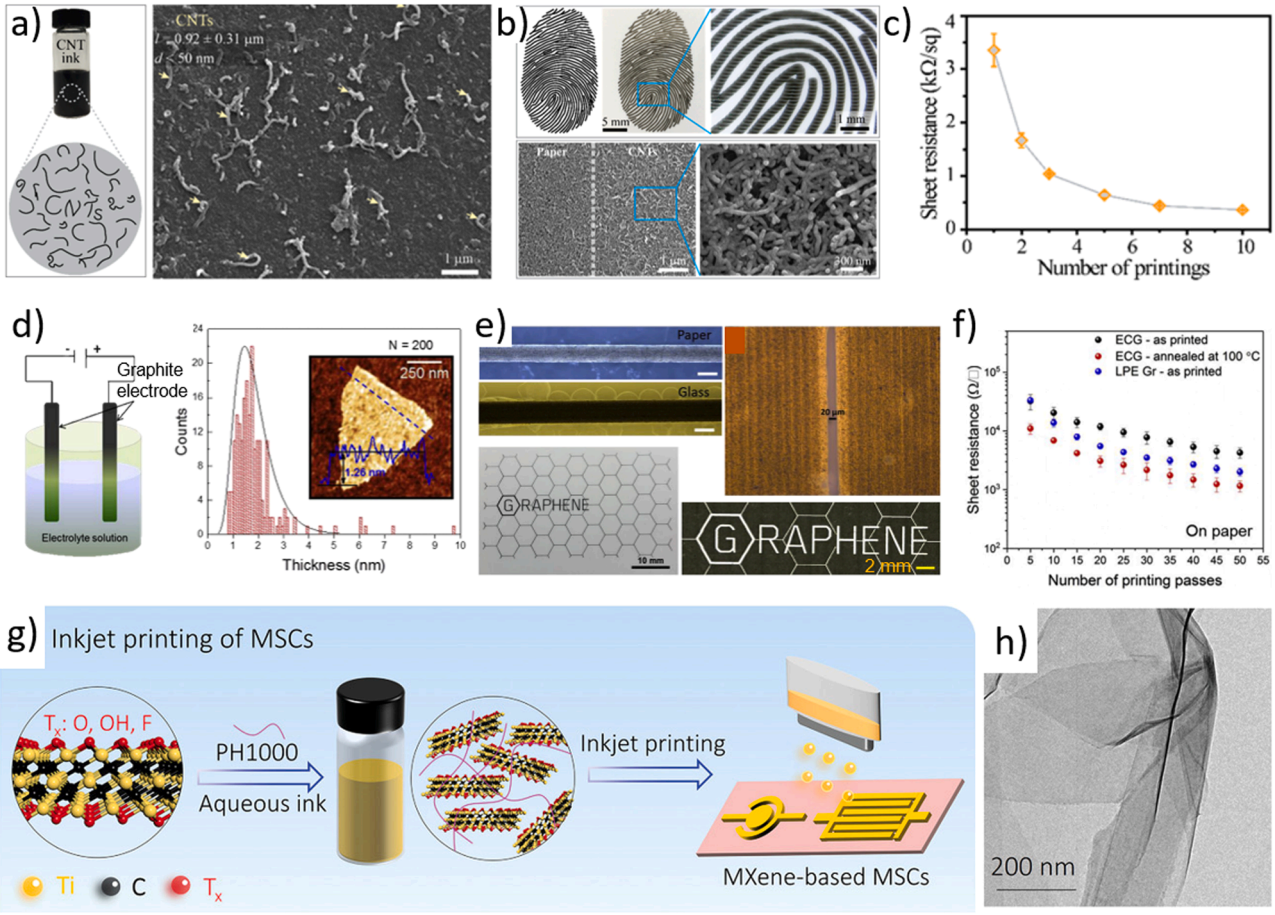

Fig. 4. **a)** Dispersed CNT ink for inkjet printing and SEM image of CNTs. **b**) Printed image CNT fingerprint patterns and **c**) its electrical properties. ((a-c) reproduced from Ref. [125] d) Schematic illustration of the ECE setup and statistical thickness (a mean thickness of ~1.3 nm) derived from AFM image of 200 ECG flakes on Si/SiO_2. Inset shows the corresponding AFM image of a single ECG flake. **e)** Images of printed graphene tracks on paper and glass substrates (scale bar 200 μm), and inkjet printed 'Graphene' logo on the paper substrate over an area of 50 mm × 30 mm. **f)** Printed graphene's electrical properties on paper (d-f reproduced from Ref. [126]). **g)** Schematic illustration of the ink formulation of the aqueous MXene/PEDOT:PSS hybrid ink for inkjet printing of devices and **h)** transmission electron microscopy (TEM) image of MXene nanosheets. ((g-h) reproduced from Ref. [127]).

[132]. The applications that can be enabled by these developments range from gas sensing applications [133], to neuromodulation [129] and stretchable electronics [134] . However, there is a limited amount of knowledge with few recent investigations advancing understanding of strategies for improvement of the functional properties of printed structure [123] and the focus on environmental considerations in development of new 1D ink formulations [134].

2.3.3. 2D nanomaterial-based inks

2D materials are attracting increasing attention due to their unique electrical, mechanical, thermal, and optical properties. They can be produced using liquid exfoliation of layered crystals to be formulated into inkjet printable inks [135]. Several 2D inks have been reported, including conductive graphene [136], semiconductive WS_2 [137] and MoS_2 [138], and insulating hexagonal BN (hBN) [97]. The potential to combine conducting, insulating and semiconducting 2D materials within one heterostructure could enable precise tailoring of device performance with multiple functionalities [31]. Similar to CNT inks, the agglomeration of 2D sheets presents challenges for the inkjet process. For graphene oxide (GO) flakes, surface functionalisation with polar groups enables ink formulation without the need for surfactants [139] and printing of ultra-large GO flakes (36 μm diameter) was demonstrated [140].

To formulate graphene inks, flakes produced using supercritical CO_2 exfoliation [141], lithium tetrahydrofuran expansion [142] and liquid phase exfoliation (LPE) [143] were used. The final properties of printed layers are affected by the flake concentration, printing and curing processes and post-deposition treatment [127]. For example, graphene can be dispersed in aqueous hybrid ink formulation and in environmentally benign solvents such as ethanol, with the stabilizing polymer ethyl cellulose (1:100 graphene/EC) and a mixture of cyclohexanone/terpineol [80] to achieve a high conductivity of 3000 S m^{-1} after inkjet printing [26]. Despite several advancements in using liquid exfoliated graphene, there are still challenges. The exfoliation method requires a long process time (typically several days) and strongly affects the quality of the flakes, influencing the final properties of printed structures. In addition, the low graphene concentration (< 0.5 mg ml^{-1}) produced by LPE requires the printing of a large number of layers to produce functional films [26,41] with a good conductivity (100 S m^{-1} for ink containing 0.11 g L^{-1} annealed at 170 °C [41]). As an alternative route, electrochemical exfoliation (ECE) provides a faster process (exfoliation achieved in a few minutes) and high-quality graphene flakes (70% single- and bi-layers with large lateral size of 1–10 μm) (Fig. 4d-f) [144]. A water-based inkjet printable graphene ink with a high concentration (2025 mg mL^{-1}) was achieved using the ECE method, which allows stable jetting, quick drying (less than 10 s), good wettability on untreated substrates such as paper and glass with high electrical conductivity (3.91×10^4 S m^{-1}) [144].

The conduction mechanism in inkjet-printed graphene structures arises from inter-flake tunnelling and a recent study showed the packing fraction of the flakes in the printed structure determines the overall conductivity [26]. Nevertheless, further studies are needed to understand the effect of flake size and residues of additives and solvents on the electrical properties of inkjet printed graphene networks.

Other 2D layered materials, including hBN [143] and transition metal dichalcogenides (TMDCs) (MoS_2, $MoSe_2$, WS_2, WSE_2) [145,146], have also been produced by liquid-phase exfoliation for inkjet printing inks. Hexagonal BN is a high-quality insulator and TMDCs are semiconductors with a desirable bandgap from 1 eV to 2 eV and beyond. The inks of these 2D materials are formulated with similar strategies discussed for graphene. Worsley et al. [97] achieved a fully inkjet-printed graphene/hBN/graphene capacitor on a flexible substrate. In searches for other 2D crystals with promising mechanical and electrochemical characteristics, in addition to electrical characteristics, transition metal carbides (TMCs) have been investigated. Wu et al. [147] demonstrated that the stability of $Ti_3C_2T_x$ MXene, produced by in situ etching, can be retained for >80 days by incorporating ascorbate ions as capping- and anti-oxidizing agents at ambient temperature. An aqueous inkjet printable MXene/PEDOT:PSS hybrid ink offers remarkable printability with adjustable viscosity, long-term stability and high volumetric capacitance (754 F cm^{-3}) due to enhanced interlayer contact in the MXene via the PEDOT:PSS layer [127] (Fig. 4g,h).

2.4. Composite inks

Within a composite ink, two or more materials are combined to produce a multifunctional hybrid possessing tailored properties which surpass those existing in the singular, separate components [148]. Composite multifunctionality is often achieved via a matrix-filler system, in which the matrix is chosen to match the processing requirements for printing and to ensure the stability and support of micro- or nanoparticulate filler materials, whilst these fillers provide functional properties [149]. The need for flexible and biocompatible electronics, as well as reuse of 3D electronics with integrated dielectric and conductive materials demand versatile materials that can deliver enhanced performance. Therefore, composite materials have become widely utilised, as they can offer a combination of desirable properties within the single material system or device.

Conductive inks containing carbon-based Ag composites are extensively explored, where small amounts of the metallic additive typically improve conductivity whilst maintaining the low-cost benefits of using carbon-based ink. For example, Ag/reduced GO (rGO) inks employing simultaneous GO reduction and Ag NP deposition have been demonstrated, with PVP acting as both a reducing agent and stabiliser [150]. The addition of spherical Ag NPs increased the conductivity of the rGO layer from 800 S m^{-1} to 2000 S m^{-1} in addition to improving the rGO dispersibility. Conductive and transparent films with improved stable conductivity were demonstrated for rGO composites with Au-decorated Ag nanotriangle platelet additives [151]. The conductive properties of composites comprised of graphene nanoplatelets and reactive Ag precursors were tuned by post-deposition reduction treatments and Gr content adjustment [152].

Achieving conductive layers can be damaging for some flexible and stretchable substrates [153], whilst metallic films are prone to cracking and interfacial delamination when subjected to stresses [154]. Matrix-filler composites, where a flexible and/or stretchable matrix is rendered conductive through the incorporation of fillers to create percolation pathways are proposed as a potential solution. Ag nano-colloids in water-based UV-curable resins were shown to have good curability and adhesion to flexible Kapton polyimide substrates [155]. AuNP/PEDOT:PSS core-shell composites have been proposed for sinter-free electrodes with increased stability during bending on paper substrates [156] and PEDOT:PSS has also been combined with small-molecule ionic additives acting as stretchability and electrical conductivity enhancers [82], and with polyurethane [157]. PDMS-based stretchable electrodes are also commonly used. Nanocomposites based on vertically grown CNTs within an inkjet printed PDMS matrix demonstrated stable performance as serpentine electrodes (Fig. 5a-c). Likewise, Ag nanowires have been embedded into PDMS, yet only the nanowires are inkjet-printed, either via direct-deposition into the liquid elastomer [158] or by the coating of PDMS onto previously-defined Ag inkjet patterns [159]. The combination of an elastomeric PDMS matrix with the conductive Ag filler at the ink formulation stage is yet to be achieved and could enable the fabrication of fully inkjet-printed, free-standing, and stretchable electrodes.

Composite inks with polymeric matrix and ceramics (e.g., barium titanate $BaTiO_3$) filler have been developed, in which the ceramic filler improves the permittivity and thus increases the polarizability of the flexible and solution-processable polymer [162]. Barium strontium titanate (BST) ceramics were surface modified and successfully formulated into composite inks with poly(methyl methacrylate) (PMMA) [163] and with flexible poly(ethylene glycol) diacrylate (PEGDA) [164]

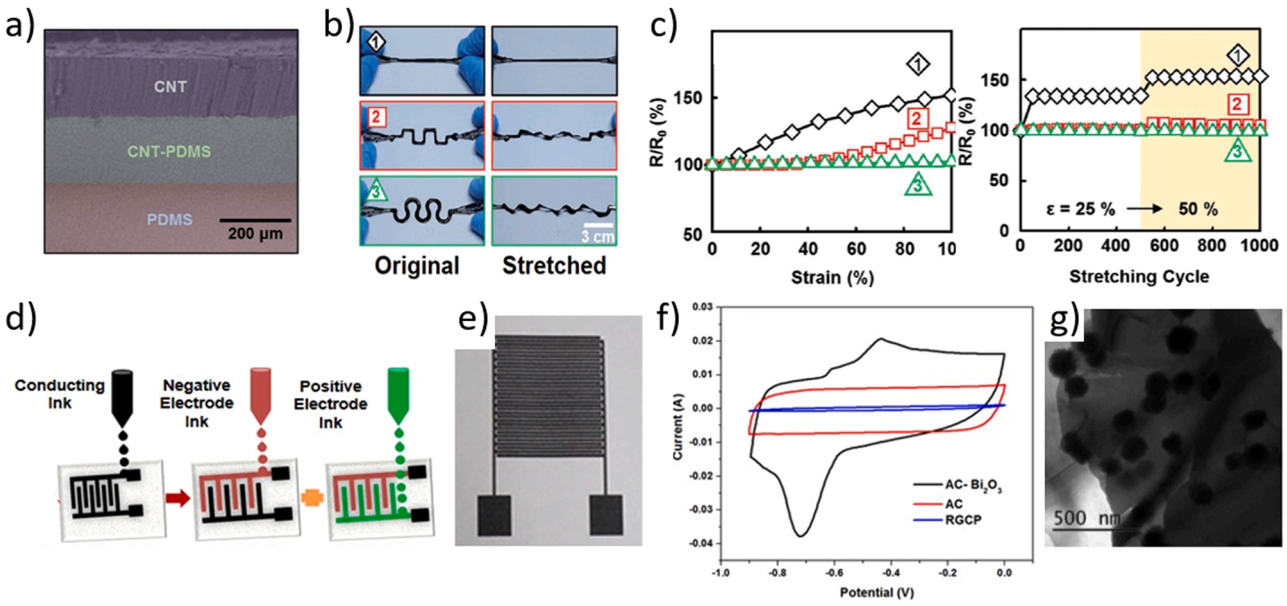

Fig. 5. **a)** Cross-section TEM image of the structure incorporating vertically grown CNTs into PDMS for composite stretchable electrodes. **b)** Photographs of the CNT-PDMS electrodes with varying designs are shown as prepared and under stretching. **c)** Resistance changes of the same electrodes in response to strain (left) and after 1000 stretching cycles (right). ((a-c) reproduced from Ref. [160]). **d)** **S**chematic and **e)** photograph of the interdigitated structure of the inkjet-printed nanocomposite electrodes as employed in supercapacitor devices. **f)** CV curves measured activated carbon (AC), AC-Bi_2O_3 and reduced graphene oxide conducting paper (RGCP) used as a reference, and **g)** TEM image of the AC-Bi_2O_3 composites ((d-g) reproduced from Ref. [161]).

to achieve homogeneous printed layers with improved permittivity in comparison to the organic materials alone. Polyvinylidene fluoride (PVDF) is a dielectric polymer with a large relative permittivity [165] but with poor solubility [166], and as such, PVDF was combined with poly(viny alcohol) (PVA) in an all-polymer composite, where the PVA serves to improve the stability as well as breakdown strength of the composite film [167]. Barium titanate ($BaTiO_3$)/epoxy thermoset composites were proposed as mechanically-stable ceramic-based layers within inkjet-printed flexible energy harvesters, taking advantage of the piezoelectric properties of $BaTiO_3$ [168]. Combined $BaTiO_3$-PVDF composite inks [165] are also used as piezoelectric hybrid materials, however, not all crystalline phases of PVDF can exhibit piezoelectricity, and in this case, the barium titanate nanofillers act as nucleating agents to encourage and stabilise the formation of the piezoelectric PVDF phase.

Composite inks such as Bi_2O_3/activated carbon (AC) and rGO/MnO_2 offer a high surface area for charge storage and a porous structure presenting pathways for the control and diffusion of ions are required in addition to high conductivity, desired in supercapacitor electrodes (Fig. 5d-g). Bi_2O_3 is of particular interest throughout literature as a filler within such applications due to its high theoretical capacitance (>1300 F g^{-1}) [169]. Similarly, rGO/MnO_2 composites are frequently used, with the MnO_2 providing high capacitance and the rGO flakes acting as large-surface-area conductive binders [170]. Other examples of composite materials used in this field include MnO_2 combined with conductive Ag/CNTs [171], rGO added to MoO_3 [172], and a combination of Gr-based materials with PANI, including rGO [173], and Gr hydrogels [174], with the composites in each case showing improvements in electrical properties as well as cycling stability when compared with the individual materials.

MXene-based composites, combining titanium carbide MXenes and Ag were formulated [175], in which the MXene provides a large surface area and hydrophilicity, whilst the Ag increases the conductivity for sensing applications. Similarly, humidity-sensitive MoS_2/PVP composite inks were optimised for jetting [176]. In these examples, exposure to moisture leads to changes in the electrical properties of the composite, thus providing the sensing mechanism, with the PVP further serving as a stabiliser for the exfoliated MoS_2 flakes in the latter case, which in turn increase the surface area available for water adsorption.

Composite materials comprised of a polymeric matrix with CNT fillers are also increasingly explored as they provide sensitivity to chemical environments [177]. Polymer layers can swell in response to volatile organic compounds, leading to disruption in the conductive network of the matrix, altering the distance between the percolating CNTs and changing the electrical properties. Several ink-jettable CNT/polymer composites have been developed [177], including CNT-PEDOT:PSS [178] used as an ethanol detecting layer, where the ethanol adsorption affects the carrier density within both the CNTs and the PEDOT:PSS, thus enhancing the sensing performance. Other chemical sensing composites include CB fillers in a SEBS matrix [179] and a semiconducting CdSe QD/polymer ink [180].

Furthermore, Gr flakes were added to Ag NP inks, producing a conductive hybrid material for strain sensor applications on PVA substrates [181]. Gr was also used with iron oxide NPs to fabricate inkjet-printed composite strain sensors with magnetic self-healing properties on polyurethane substrates [182], and ZnO NPs were added to Gr for PDMS-based stretchable strain gauges [183]. In each of these examples, the use of fillers improves the connectivity between adjacent graphene flakes, thus enhancing material performance.

From this review of the recent work, the opportunities offered by the composite material are clear, particularly those arising from control of functional properties enabled by composite composition [148]. However, changes in composition have significant effect on the rheology of the inks and the jettability [177,178] of the composite materials, hence optimization is required for every iteration of ink composition. From the review of the literature, the polymer-nanoparticle composites are emerging as potentially viable for electronics, where the tunability of nanomaterial properties can enable control of function, while requiring minimal changes to formulation and AM deposition process [149,176,182]

2.5. *Advantages and disadvantages of different functional inks*

To enable inkjet of electronic devices, inks of functional materials with differing properties are needed. Polymer-based, nanomaterial-based and composite inks, summarised in this review, offer

complementary advantages. Polymer-based inks, for instance, offer an economical option and stable jetting (with minimal nozzle clogging compared to filler-based inks), along with good substrate adhesion [22,66]. However, limited mechanical strength and poor stability of thermal and electrical properties can present challenges [22–25]. In contrast, nanomaterial-based inks, such as metal nanoparticles, offer advantageous stable electrical conductivity, strong mechanical properties and excellent thermal stability [27–29]. However, high sintering temperatures (>150 °C [85,89]) add complexity to post processing procedures, while high material costs [28] can limit their use. Carbon-based nanomaterials, such as CNTs and graphene, are lightweight and environmentally benign solutions as electrically conductive materials, however optimization of the formulations is needed to increase shelf life of the device [26,118]. In addition to the aforementioned inks, inkjet printing of single-crystal films, such as organic semiconductor 2,7-dioctyl[1]benzothieno[3,2-*b*][1]benzothiophene (C_8-BTBT) have been explored. Such single crystal materials can be printed in ultrathin and scalable arrays for high-performance electronic devices [184,185].

Composite inks on the other hand can integrate the advantages of both polymers and nanomaterials but require intricate formulation, and the resulting ink properties can fluctuate significantly based on composition, hence further research is needed in this area. Availability of inks with different properties can address the needs for specific intended application. For instance, polymeric inks are more suitable in applications such as wearable electronics, where higher electrical conductivity is not demanded, or even can be used as a dielectric layer. Nano-dimensional inks are suitable where enhanced conductivity and mechanical robustness is required, such as energy storage devices and sensors [87,88]. Carbon based inks could be considered for various sensing applications including biomedical fields [118,125]. Composite inks present a viable option for harnessing the benefits of both material types such as stretchable and flexible electronics [148,177].

3. Inkjet-printed devices

Inkjet printing provides unique benefits for manufacturing electronic devices, allowing for high-performance heterostructures and planar structures through drop-on-demand and non-contact deposition. This includes the fabrication of thin (< 100 nm) uniform films and tall (> 1 mm) structures on various surfaces (e.g., rigid/flexible planar and conformal) for large-area manufacturing and the next generation of 3D electronics.

3.1. High resolution printing of conductive patterns

Achieving high accuracy deposition and high-resolution patterns is paramount for electronics. Significant efforts have been invested into optimisation of inkjet printing, particularly printing of conductive patterns. Typically, resolution is limited by the size of an individual droplet and the positioning accuracy of the printing equipment. A number of approaches were developed in order to achieve high resolution [186], including optimisation of ink formulation [184,187], altering the wetting properties of the substrate [188], and optimising printing process and developing strategies for higher pixel packing density [189]. Ink formulations of metal nanoparticle inks and conductive polymer inks were optimised to control the droplet formation and spreading on the substrate [22,27,28,76]. Printing strategies have been constantly looked at, showing that close arrangement of droplets/pixels by reducing the drop spacing can lead to higher-resolution and high-definition features [187,190]. Inkjet deposition of soluble sacrificial layers have also shown to be advantageous for deposition of high-resolution metal patterns [191]. Most of the work to date in this area is advantageous for printed 2D electronics, however the challenges associated with achieving high positioning accuracy for multiple layer deposition remains to be fully resolved. High-content and high-viscosity conductive inks [192,193] and other AM processes, such as multi-photon polymerization [194], are explored for printing conductive 3D structures, however further work is needed to fully understand the opportunities.

3.2. Printed optoelectronic devices and sensors

Optoelectronic devices such as solar cells, and LEDs can be fabricated on curved and flexible substrates for wearable and healthcare devices. However, several challenges such as the deposition of thin uniform layers and the intermixing of materials that often occurs in printed heterostructures still need to be considered.

3.2.1. Solar cells

Compared to spin-coating, inkjet printing offers the potential for fabricating larger area solar cells with higher throughput rates and less material wastage [195]. Inkjet printed solar cells could offer enhanced performance, as was demonstrated for conventionally manufactured dye-sensitised solar cells, where the conventional platinum (Pt) counter electrodes were replaced with cost-effective and flexible inkjet-printed graphene [196]. A high power-conversion efficiency (PCE) was achieved, corresponding to ~70% of the PCE achieved in drop-cast Pt devices at ~3% of the material cost. The performance of conventional Si solar cells can also be enhanced by surface decoration with an inkjet-printed anti-reflective porous layer of silicon (Si) QDs. Inkjet printing here enabled low-waste deposition while also allowing for control of the thickness and porosity of the QD film, resulting in a 15% increase in external quantum efficiency in the 300–400 nm wavelength range [197].

In recent years, a record PCE of 22.1% [198] was reported for solar cells with a spin-coated perovskite photoactive layer. To achieve scalability and customisation, inkjet-printed perovskite ($MAPbI_3$) photoactive layers were inkjet-deposited with the layer thickness controlled by the printing strategy and crystal size tuned by a vacuum annealing step [199]. The resulting device displayed a PCE of ~11%, comparable to that achieved in spin-coated devices. Solar cells incorporating inkjet-printed triple cation $Cs_{0.1}(FA_{0.83}MA_{0.17})_{0.9}Pb(Br_{0.17}I_{0.83})_3$) perovskites with improved temperature and moisture stability [200] displayed PCEs up to 12.9% and were shown to withstand temperatures of 80 °C for 120 min with a small decrease in PCE of ~10%. To further enhance device performance, greater control over the NP crystallisation process is required [200].

Despite demonstrating lower PCE than perovskite solar cells, organic devices offer the benefits of being fully inkjet-printed and are well-suited for applications in wearable and healthcare electronics [25,201]. In these devices, semi-transparent electrodes were achieved with PEDOT:PSS and a silver grid [201], and the solar cells were fabricated in an ambient atmosphere with an area >1 cm^2 and PCE = 4.1%. Fully inkjet-printed indium tin oxide (ITO)-free, ultrathin, lightweight organic solar cells (Fig. 6c,d) on biocompatible parylene substrates was demonstrated with PCE = 3.6%.

3.2.2. LEDs

Along with solar cells, the integration of optically active materials with the inkjet-printing processes has enabled the fabrication of photoluminescent films, lasing devices, and LEDs [204,205]. The complex patterns enabled by inkjet deposition make it a particularly attractive method display applications. Also, the unique and random drying behaviour of each droplet [206] enabled the fabrication of unclonable security labels and full-colour converter films for LEDs using inks of $Zn_xCd_{1-x}Se_yS_{1-y}$ QDs encapsulated by NaCl crystals [206]. QD films with optical emission in the red, green, and blue wavelength ranges of the electromagnetic spectrum were sequentially inkjet-printed onto PET (polyethylene terephthalate) substrates to fabricate flexible full-colour RGB QD@NaCl convertor films for full-colour displays with a pixel size of 3.74 ± 0.5 μm [206].

Photoactive materials have also been printed in LED structures. For example, a small-molecule organic material 1,1′-(9,9-bis(4-(hexyloxy)

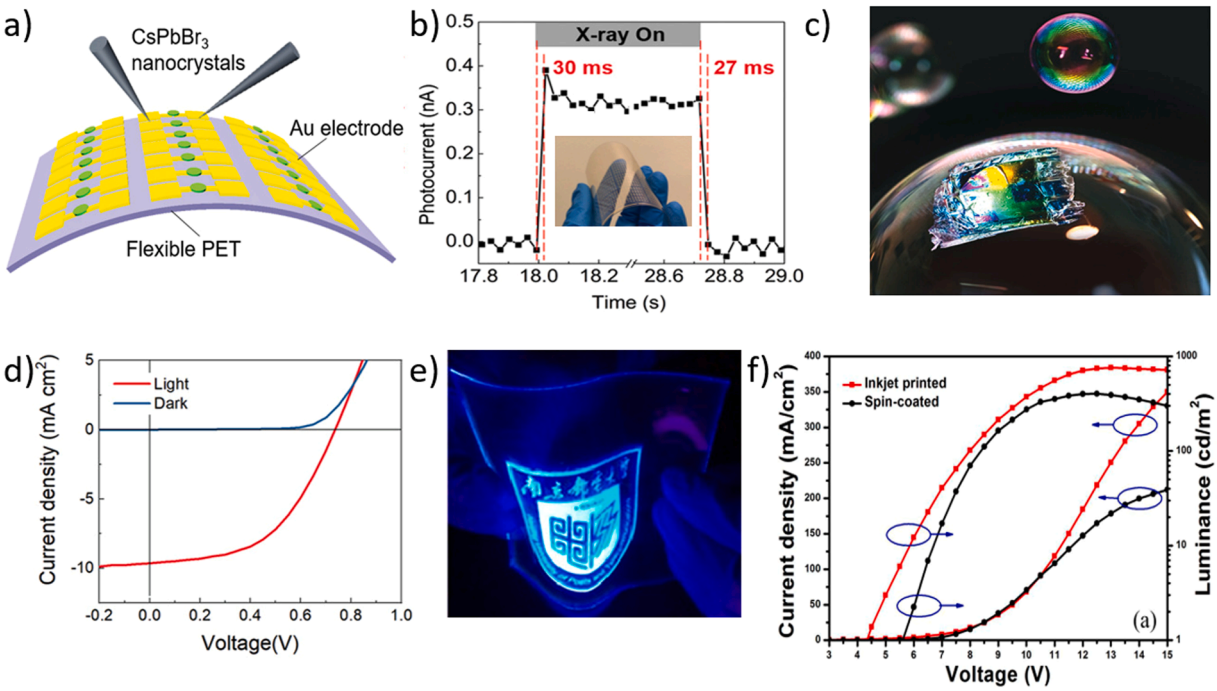

Fig. 6. a) Schematic diagram of an X-ray detector based on an inkjet-printed perovskite QD photoactive layer and **b)** temporal dependence of the photocurrent induced in the device by incident X-rays with response times of ~30 ms. Inset shows a photograph of an array of these photodetectors on a PET substrate ((a-b) reproduced from Ref. [202]). **c)** Photograph of an ultralightweight fully inkjet-printed organic solar cell suspended on a soap bubble and **d)** dependence of the current density of the solar cell as a function of voltage in dark and light conditions ((c-d) reproduced from Ref. [25]). **e)** Photograph of a blue organic LED with an inkjet-printed emissive layer on a flexible transparent substrate and **f)** the luminance and current density of this device are shown to be superior to that of a reference device deposited by spin coating ((e-f) reproduced from Ref. [203]).

phenyl)−9H-fluorene2,7-diyl)dipyrene (PFP-3) was inkjet-printed as an emissive layer in an LED to produce large-area light-emitting flexible patterns (Fig. 6e,f), with a luminance of 800 cd m^{-2} at 13 V and maximum current efficiency of 0.6 cd A^{-1} [203]. LEDs were also reported with an inkjet-printed CdSe/ZnS QD emissive layer [207], where coffee-ring-free and low-roughness QD films were achieved using a mixture of dodecane and cyclohexylbenzene solvents. The fabricated LEDs displayed a low turn-on voltage of 2.0 V, a luminance of 12,100 cd m^{-2} at 12 V, and a maximum current efficiency of 4.44 cd A^{-1}.

More recently, metal halide perovskites have attracted considerable attention for LED applications due to their high quantum yields and tolerance to defects. Hammerschmidt et al. [204] developed a method to directly control the crystallisation of inkjet-printed perovskite composites ($MAPbBr_3$:PEG) and achieved the first inkjet-printed perovskite emissive layer in an LED. This was performed by blending a PEDOT:PSS hole injection layer with KCl to create a seeding template for the inkjet-printed perovskite layer. The inclusion of KCl in the PEDOT:PSS increased the luminance of the device by a factor of 20, achieving a maximum luminance of 4000 cd m^{-2} with a turn-on voltage of 2.5 V.

Charge carrier-transport materials such as ZnO [212], PEDOT:PSS [213], PVK [214], and poly-TPD [78] have been also printed, though the fabrication of fully inkjet-printed devices remains to be achieved for several reasons. As with inorganic solar-cells, LED devices require the deposition of several layers on top of one another, each with a uniform thickness of ~50 nm [215], which is still challenging via inkjet printing and further work on the formulation of inks and their integration with the deposition process is needed. Also, the deposition of heterostructures for photodetectors, solar cells, or LEDs can lead to intermixing between layers [216], which further affects the ability to control the layer thickness and/or the quality of the interface.

3.2.3. *Optical synaptic devices and memristors*

The synapse is one of the fundamental elements in the human brain for performing functions such as learning, memorising and visual processing. There has been a growing interest to develop optical synaptic devices that mimic the biological synapses using inkjet printing. Graphene and Ag electrodes were inkjet printed to develop photo-synaptic organic field-effect transistors (OFETs) that emulate visual responses to external light [217] with ultralow energy consumption (0.07–34 fJ per event). Optoelectronic synaptic transistors based on quantum dot–metal oxide semiconductor (InP/ZnSe QDs) heterojunctions were inkjet printed and demonstrated a low power consumption (~5.6 pJ per event) for activation [218]. Likewise, inkjet printing of indium-tin-oxide (ITO) synaptic thin-film transistors (TFTs) using solution-processed high-k zirconium oxide (ZrOx) gate dielectric layer are reported [219]. Moreover, the coffee ring effect of ITO during inkjet printing is exploited to develop optoelectronic synaptic transistors [144]; a 10 × 12 coffee-ring structure with a high spatial resolution (142 dpi) with durable visual detection and memory behaviours were demonstrated.

Optoelectronic memristors are memory devices that exploit resistive switching that can be controlled both optically and electronically. Inkjet printing is a promising choice to develop resistive switching materials and devices. Various nanoparticle-based inks have been used to develop memristor devices using inkjet deposition. Metal nanoparticles are one of the promising choices where the formation of metal oxide can be used to introduce the change in resistance [220,221]. Recently, inkjet-printed memristors based on an Ag/WO_{3-x}/Au were reported with a resistive switching ratio of ~100 [222]. Similarly, graphene oxide has been inkjet printed to develop metal/insulator/metal memristor devices, although a relatively low resistive switching ratio ~ 4 was reported [223]. While this is a fast growing area of research, realistic prospects for inkjet printed devices synaptic devices and memristors can only be achieved with development of comprehensive fundamental understanding of neural networks. This multidisciplinary research is fast advancing and AM can provide an underpinning technology for its exploitation.

3.2.4. Inkjet printed sensors

Ink-jet printing enables the deposition of complex geometries, including deposition onto flexible and curved substrates, often required for sensors. To date, sensing applications have been explored ranging from chemical sensing [224] to humidity [225] and strain gauges [226]. For example, a chemical sensor was produced for measurements of enzymatic activity [227] where glucose oxidase, lactic oxidase, or mixed lipase/glycerol kinase/L-α-glycerophosphate oxidase inkjet-printed onto PANI hydrogel demonstrated respective sensitivities of 5.03, 3.94, and 7.49 μA mM^{-1} cm^{-2} [228]. An rGO-based sensor could detect concentrations of NO_2 as low as 500 ppb [229] due to the high sensitivity, although with a slow recovery time (> 30 min). Optimization of the sensing layer thickness via inkjet printing strategy can be used to balance sensitivity vs response time to improve device operation. The sensitivity of low-dimensional materials (e.g., SWCNT, Pd NPs) to the presence of nearby charges was exploited in pH meters, allowing low-cost, real-time pH monitoring [230]. Also, wearable 'electronic noses' were fabricated on PEN substrates for the detection of a variety of chemicals, such as ammonia, acetic acid, acetone and ethanol [231].

High-sensitivity photodetectors are valuable tools for a range of applications, from fire detection to advanced communications, and several devices have been developed via inkjet printing [162]. One method for manufacturing high-performance photodetectors is the surface decoration of single-layer graphene with inorganic nanomaterials. This has been achieved using HgTe QDs [232] and perovskite nanocrystals [32] with responsivities up to 10^6 A/W. These devices had sensitivity ranges tuneable by nanocrystal content and inkjet printing enables the fabrication of different devices on a single silicon (Si) chip. This is not possible with other coating techniques such as spin coating and thus paves the way for advanced sensing devices with multiple detectors sensitive to different wavelengths on a single chip.

Fully inkjet-printed photodetectors are ideal for wearable electronics as they can be easily manufactured on flexible substrates and personalized for individuals. To date, fully inkjet-printed photodetectors have been demonstrated with a variety of materials. Ag NPs were deposited onto ZnO films for UV detection [233], where surface plasmons of metal NP enhanced the photocurrent of the device, achieving a detectivity of 1.45×10^{10} Jones at 0.7 mW incident light power. Semi-transparent PEDOT:PSS electrodes were used in combination with a photoactive layer of small organic molecules 7,7′-(4,4-bis(2-ethylhexyl)−4H-silolo [3,2-*b*:4,5-*b*′]dithiophene-2,6-diyl)bis(6-fluoro-4-(5′-hexyl-[2,2′-*bithiophen*]−5-yl) benzo[*c*][1,2,5] thiadiazole) (T1), [6,6]-phenyl--C_{70}-butyric acid methyl ester ($PC_{70}BM$), and P3HT [234] were used in a broadband photodetector with both sides photosensitive and an external quantum efficiency above 10%. Fully inkjet-printed photodetectors with tuneable response and high photoresponsivity (up to 10^2 A/W) were achieved for graphene/perovskite detectors [32]. X-ray detectors were fabricated from all-inorganic metal halide perovskite QDs ($CsPbBr_3$) deposited onto PET and Si/SiO_2 substrates with gold counter electrodes pre-deposited via photolithography [202]. Compared to conventional α-Se devices, these devices were 70 times more sensitive with a fast response time of 30 ms at a low bias voltage of 0.1 V (Fig. 6a, b).

Inkjet-printing is scalable to arrays of sensors as well [235]. A grid of sensing capacitors was produced with the layout and resolution of industry-standard touchscreens [236] and stable operation at a curvature as low as 8 mm using poly(methylsiloxane) dielectric, silver connectors and flexible PEDOT:PSS electrodes. Inkjet-printed silver electrodes with a size and shape optimised for maximum sensitivity were used in capacitors to measure pressure fluctuations [237] and the precise position of a moveable mirror in a spectrometer [238].

To date, the most common printed mechanical sensors are strain gauges. A sensitivity, or gauge factor (GF), of 2.77 [239] was demonstrated in inkjet-printed carbon nanotubes by rotating the printing direction 90° between layers to improve film uniformity, whilst a high GF of 165 was reported for a graphene-PEDOT:PSS sensor [226]. Novel types of strain gauges exploit the exponential dependence of the tunnelling current on the distance between un-sintered nanoparticles, resulting in a GF of 60 over a wide range of applied strains [208]. The coffee ring effect was exploited to create 5 μm wide traces of Ag nanoparticles and the device performance was reproducible over repeated loading-unloading cycles (Fig. 7a). A strain gauge functionalised with heart-muscle cells was found to be responsive to those cells flexing (Fig. 7b) [224], reliably detecting changes in the heartbeat in response to drugs. It can hence be employed as an implant for real-time monitoring in drug trials.

Humidity monitoring with gravimetric sensors was achieved with inkjet-printed GO films [210]. An array of GO capacitors in a micro-machined ultrasonic transducer was produced such that water absorption into the graphene changed the resonant frequency of the array due to increased mass (Fig. 7c). The high surface-to-volume ratio of 2D materials and the presence of hydrophilic edge sites is beneficial for humidity sensing, and sensors were successfully fabricated using 2D MoS_2 with PVP [176], and titanium MXene functionalised with Ag on a flexible PEN substrate [175]. Inkjet-printed interdigitated silver electrodes on paper enabled cost-effective and flexible humidity sensors [240], where a change in the resistivity or dielectric constant of paper upon water absorption is recorded. The sensitivity of metallic ink layers to temperature enables simultaneous temperature and humidity sensing, however discriminating between signals due to different factors can be challenging. A dedicated temperature sensor with high sensitivity (2.23×10^{-3} C^{-1}) on a flexible polyimide substrate was demonstrated with Ag NPs [241], with other examples utilising carbon nanoparticles and PEDOT:PSS (3.9 mV C^{-1}) [242], or graphene and PEDOT:PSS (0.6×10^{-3} C^{-1}) [243].

3.3. Inkjet printed energy storage devices

Energy storage devices include capacitors, supercapacitors, batteries, and fuel cells. They all require materials with large surface areas, which inkjet printing is ideally suited to produce. In this section, we look at the variety of materials and geometries that have been produced, focussing on high-performance or unique designs that cover the range of technologies that inkjet printing enables.

3.3.1. Capacitors and supercapacitors

Parallel plate capacitors contain a dielectric material sandwiched between two electrodes: ceramic/polymer $Ba_{0.6}Sr_{0.4}TiO_3$ (BST) and poly (methyl methacrylate) (PMMA) composites were used with silver electrodes [163] and displayed dielectric constants between 20 and 55 at 1 kHz. Fully-inkjet-printed capacitors consisting of 2D graphene electrodes were successfully demonstrated with 2D hexagonal boron nitride (hBN) as a dielectric material (Fig. 7d) [97]. These devices achieved an areal capacitance of ~2 nF cm^{-2} (Fig. 7e).

Supercapacitors typically include two electrodes, an active electrolyte, and a separator, with the electrode material being the most important component. Supercapacitor electrodes must possess a high surface area for charge storage and a porous structure to present pathways for the diffusion of ions during the charging/discharging process [244]. Carbon-based matrices and metal oxide fillers, such as CNT and UV-cured triacrylate-polymers [211] (Fig. 7f), were used in fully inkjet-printed supercapacitors on paper, which displayed an areal capacitance of 100 mF cm^{-2} stable over 10,000 charge/discharge cycles. Flexible supercapacitors consisting of inkjet-printed rGO and MoO_3 composite electrodes in a poly(vinyl alcohol) (PVA)-H_2SO_4 solution achieved a high volumetric specific capacitance of 22.5 F cm^{-3} at 0.044 A cm^{-3}, with a capacitance retention rate of 82% after 10,000 charge-discharge cycles [172]. Similarly, inkjet-printed rGO/MnO_2 composite supercapacitor electrodes were demonstrated for self-powered sensor systems on flexible substrates for wearable wristband applications [170]. The printed supercapacitors displayed an areal capacitance of 12.9 mF cm^{-2} at 0.12 mA cm^{-2}, with a capacitance retention rate of 80% after 2500 charge-discharge cycles. Several groups

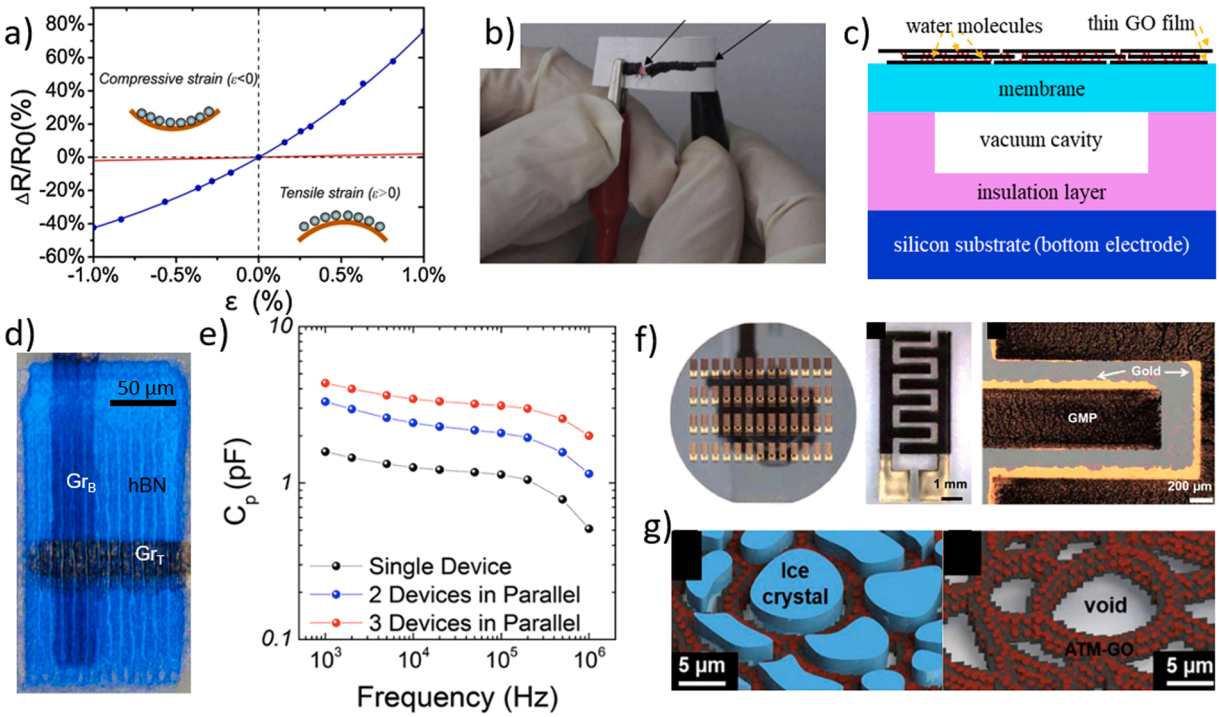

Fig. 7. **a)** The exponential gauge factor of the strain gauge made from the nanowires (blue) and a commercial metal foil strain gauge with a gauge factor of 2 (red) for comparison (reproduced from Ref. [208]). **b)** Inkjet-printed graphene strain sensor on a paper substrate under tensile compressive strain. (reproduced from Ref. [209]) **c)** Schematic of a cross-section of a single resonance cavity used in a humidity sensor. The inkjet printed graphene layer absorbs water, increasing the mass of the Si_3N_4 membrane, and altering the resonant frequency. SiO2 is an insulating layer (reproduced from Ref. [210]). d) a Photograph of a fully inkjet-printed capacitor with graphene top and bottom electrodes, and an hBN dielectric layer, and **e)** the capacitance of these devices as a function of the frequency ((d-e) reproduced from Ref. [97]). **f)** Inkjet-printed doped passivated graphene flakes (GMP) micro-supercapacitors (MSCs) with printed gold current collectors and GMP electrodes. From right to left: Photograph of printed on a 4-inch Si wafer and micrographs of a printed device (40 GMP layers) on glass. (reproduced from Ref. [211]). **g)** Schematic of ice crystal formation in an ink droplet on the impact on a print-bed with temperature $T = -30$ °C and (right image) a highly porous MoS_2/GO anode formed by freeze-drying of the structure (reproduced from Ref. [138]).

report the combination of Gr-based materials with PANI for inkjet-printed supercapacitor electrodes [173]. PANI-Gr hydrogel composite electrodes were employed within fully inkjet-printed, free-standing, macroscopic supercapacitor devices supported by a 'graphene paper' which demonstrated a specific capacitance up to 307 F g^{-1} at 0.2 A g^{-1} and maintained 90% capacitance after 1000 charge-discharge cycles [174]. Inkjet printing was used to deposit pseudocapacitive additives onto supercapacitor electrodes to enhance capacitance, such as bis-terpyridyl-based molecular cobalt complexes on laser-induced graphene films separated by a LiCl/PVA solid electrolyte [245]. The areal capacitance of the device was enhanced by a factor of 75 to ~0.8 mF cm^{-2}.

3.3.2. *Batteries and fuel cells*

A battery contains two electrodes – the anode and the cathode – at which redox reactions take place to provide current to an external load, which are separated by an electrolyte. Lithium-based batteries provide excellent capacity and low density, hence a number of lithium-based inks have been formulated to print cathodes [246] and were further functionalised with allotropes of carbon, such as carbon nanotubes (CNT) [247] or carbon black (CB) [248], to improve their conductivity. The beneficial performance of composite materials as electrodes in batteries has been demonstrated using CNTs with straight-chain sulphur for lithium-sulphur batteries [247], and PEDOT:PSS with silicon nanoparticles (Si NP) and CB for lithium-ion batteries [248]. These electrodes offer high theoretical capacity, reduced cracking, enhanced cycling stability, improved conductivity, and mechanical and chemical stability, and PEDOT:PSS acts as a binder to prevent damage due to the volume expansion typically seen upon Li-ion insertion.

Porosity can also be improved by using naturally microporous materials, such as $LiFePO_4$ particles [249] and $LiMn_{1-x}Fe_xPO_4$ [250]. A freeze-drying process was used to introduce macropores in a MoS_2 and rGO composite by printing onto a substrate plate at -30 °C, producing a porous anode for a sodium-ion battery [138] (Fig. 7g). The MoS_2 provides a layered structure to facilitate ion intercalation and the rGO improves the conductivity of the printed electrodes. Table 2 shows the specific capacity of the batteries discussed here. To date, each part of a battery has been individually realised by ink-jetting, but an entire battery is yet to be achieved, primarily due to the challenge of adequate encapsulation [251]. Also, further improvements in power- and energy densities are needed and can be achieved by enhancing the performance of materials and the printing resolution for the development of micro-batteries as well as wearable or even implantable energy storage devices in the future.

Fuel cells require a continuous supply of fuel and oxygen to produce power without the need for a recharging process. Similarly to batteries, many of the individual components have been successfully inkjet-printed [258,259]. The first fully-printed hydrogen fuel cell was reported recently with laser-produced holes in the substrate to allow for fuel supply [260]. Despite the limited ability of inkjet printing to manufacture the hollow structures required for the fast delivery of reactants and removal of waste products from fuel cells, this work demonstrated the potential of inkjet printing for the deposition of all active layers required.

3.4. *Fully inkjet printed integrated electronics toward 3D electronics*

The primary benefit of inkjet printing is its ability to facilitate the multi-material inkjet-based 3D printing (MM-IJ3DP) process, which incorporates multiple DOD printheads within a single machine. This

Table 2
Commercial and state-of-the-art inkjet printed devices and their performance parameters. Material deposited using inkjet printing are indicated with tick (✓).

Commercial and state of art technology or devices	Materials	Printed	Properties/Performance Specific Capacity (C_p), Discharge rate (Q), No of cycles (N) and notable features	Ref.
Batteries	Anode: Si NPs/PEDOT:PSS	✓	$C_p = 2500$ mAhg^{-1}, $Q = 0.1$ C, $N = 1$	[248]
	Cathode: Li foil	-	$C_p = 1000$ mAhg^{-1}, $Q = 0.1$ C, $N = 1000$	
	Electrolyte: 1 M $LiPF_6$	-		
	Anode: Li foil	-	$C_p = 800$ mAhg^{-1}, $Q = 0.1$ C, $N = 100$	[247]
	Cathode: Li-S/S@SWNT	✓		
	Electrolyte: 1 M $LiCF_3SO_3$	-		
	Anode: Li foil	-	$C_p = 800$ mAhg^{-1}, $Q = 9$ C, $N = 100$	[250]
	Cathode: $LiMn_{0.21}Fe_{0.79}PO_4$@C Electrolyte: 1 M $LiPF_6$	✓	$C_p = 150.2$ mAhg^{-1}, $Q = 10$ C, $N = 1000$ C_p: 108.4 mAhg^{-1},	
		-	$Q = 100$ C, $N = 1000$	
	Anode: Ag	✓	$C_p = 70$ mAhg^{-1}, $Q = 0.04$ C, $N =$ NA	[252]
	Cathode: Ag	✓		
	Electrolyte: 10 M KOH/ZnO	-		
	Anode: MoS_2/graphene aerogel	✓	$C_p = 429$ mAhg^{-1}, $Q = C/3.3$, $N = 10$	[138]
	Cathode: Sodium	-		
	Electrolyte: 1 M $NaClO_4$	-		
	Anode: $Li_4Ti_5O_{12}$	-	$C_p = 60$ mAhg^{-1}, $Q = 0.1$ C, $N = 100$	[253]
	Cathode: $LiFePO_4$	-		
	Electrolyte: Silica ionogel	✓		
PCBs from Elephantech	Substrates: PET, PI	-	Min trace width: 150 μm	[254]
	Inks: Ag NPs	✓	Build dimension: 180 × 270 mm,1 layer Deposition: Thermal inkjet Ag NPs as nucleation points for Cu deposition	
PCBs from PV Nanocell	Substrates: PET, ITO, glass, PI	-	Trace width: 70 μm	[255]
	Inks: Ag, Au, Cu NPs	✓	Build dimension: 427 × 365 mm,1 layer Up to 10 inks simultaneously Deposition: Piezo inkjet; speed 1.1 m^2/hr	
PCBs from BotFactory	Substrates: FR4 epoxy, Kapton film, and other flexible and rigid substrates	-	Trace width: 200 μm	[256]
		-	Build dimension: 117 × 152 mm, 4 layers	
	Inks: Ag NPs, dielectric	✓	Deposition: Thermal inkjet; Integrated with the pick-and-place installation system	
PCBs from Nano Dimension	Substrates: FR4 epoxy, Si wafer, Cu foil, polycarbonate, Kapton film	-	Trace width: 80 μm	[257]
		-	Build dimension: 160 × 160, 3 layers	
	Inks: Ag NPs, acrylate-urethane	✓	Deposition: Piezo inkjet	

integration allows users to simultaneously print different materials at a minute (pico-litre) scale. Additional advantages include the co-deposition of various materials (such as conductive and dielectric inks), easy scalability, direct printing onto the desired substrate, and the production of metamaterials in a non-contact printing method. These factors collectively make inkjet printing a practical method for achieving 3D electronics [261]. The main electronic components and other accessories such as the wiring, power source, and packaging are all to be fabricated by a single process, which could be enabled by inkjet printing. To fully realise the integrated 3D electronics, multiple materials need to be printed together. Multimaterial electronics printing can be realised either by changing the ink cartridge or substrate or combining various processes. This method has been widely reported to develop vertical 3D heterostructures and planner 2D structures with various inks. This section reviews advancements in the fabrication of fully inkjet-printed transistors and printed circuit boards (PCBs) and 3D inkjet-printed electronics. Further, we discuss the requirements and progress in multi-material inkjet 3D printing (MM-IJ3DP) towards fully 3D-printed integrated electronics.

3.4.1. Transistors

Fully inkjet-printed transistors have been a major focus of study in recent years [262,263]. Field effect transistors (FETs) were demonstrated in a vertical heterostructure configuration, where inkjet printing enabled the simultaneous deposition of the silver source and drain electrodes with an isolated organic semiconductor layer (Poly[2,5-bis(alkyl)pyrrolo[3,4-*c*]pyrrole-1,4-(2H,5H)-dione-alt-5,5′- di(thiophen-2-yl)−2,2′-(E)−2-(2-(thiophen-2-yl)vinyl)-thiophene] (PDVT-8)) [264]. An array of these devices was demonstrated with favourable stability and ultrashort channel lengths with current densities exceeding 6 mA cm^{-2} on both rigid and flexible substrates. The organic semiconductor P3HT was blended with the insulating amorphous polystyrene (PS) for protective encapsulation and printed as a channel material in FETs, which demonstrated maximum field-effect mobility and on/off current ratio of 0.02 cm^2 V^{-1} s^{-1} and 10^6, respectively. The structure of the printed blend films can be tuned by the composition of the solvent mixture [265]. Sholz et al. [263] fabricated fully-inkjet-printed metal-oxide (indium-oxide) thin-film transistors (TFTs) on ITO substrates with PEDOT:PSS top-gate electrodes. Inherent random variations of the surface roughness of each inkjet-printed device were exploited to generate unique identifiers for data security applications [263].

The combination of a graphene active channel, silver electrodes, and an hBN dielectric layer was used to realise fully-inkjet-printed FETs [26] (Fig. 8b). Depth profiling and 3D mapping revealed that the printed graphene layer was non-homogeneous and large intermixing of layers was present due to the inkjet printing deposition method (Fig. 8c). To account for this, the charge transport model was developed to include quantum tunnelling between graphene flakes and percolation dynamics [26]. This revealed that the electrical properties of the device are strongly influenced by the packing fraction of graphene flakes and by complex electron trajectories that traverse several printed layers, illustrating the complex transport dynamics of inkjet-printed electronic devices. At low gate voltages (<5 V), the aforementioned FETs displayed field-effect mobilities of 25 cm^2 (V s)$^{-1}$ [26] and 91 cm^2 (V s)$^{-1}$ [143]. Further miniaturization of inkjet-printed transistors is still needed, but the opportunities for customisation and integration with other processes make these devices attractive for different applications [263].

It should be noted that fabricating a single transistor device can be expanded to create 3D electronics. For example, fully inkjet 3D printed monolithic integrated flexible transistors were developed by staking

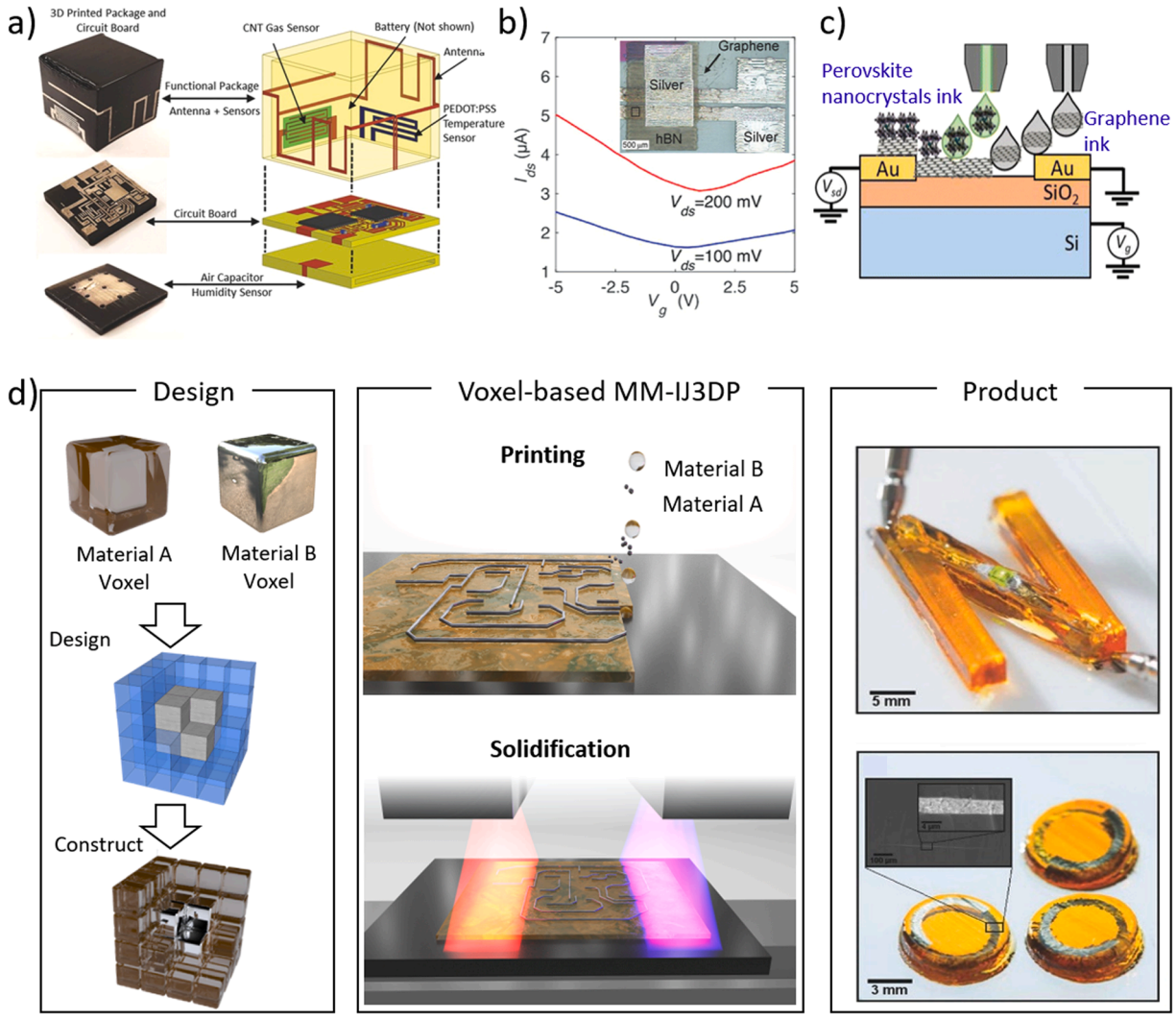

Fig. 8. a) An example of 3D electronics, optical images and schematic diagram of device assembly. The sensor node is comprised of an assembly of a 3D-printed functional package, circuit board, and air capacitor (reproduced from Ref. [266]). **b-c)** Multi-material fully inkjet printed heterostructure or planner devices towards 3D electronics, b) fully inkjet-printed planner graphene/hBN FET device (reproduced from Ref. [26]) and c) fully inkjet printed perovskite nanocrystals/graphene heterostructure photodetector device (reproduced from Ref. [32]). **d)** Voxel-based MM-IJ3DP approach. Schematic illustrating deposition of functional materials as voxels (50 ~ 100 μm) into complex 3D structures (left). The spatial distribution of each material voxel is designed to produce a target structure (middle). Photograph of a PCB device with spatially distributed spiral conductive tracks manufactured by MM-IJ3DP (reproduced from Ref. [87]) (right).

single-gate and dual-gate organic transistors [267]. Similarly, fully inkjet printed 3D integrated circuits (ICs) based on a 3D complementary organic field-effect transistor were achieved by vertically stacking a p-type OFET over an n-type OFET with a shared gate joining the two transistors [268,269]. In addition, taking advantage of the flexibility of polymeric substrates, various flexible and wearable electronic TFT devices with excellent electrical characteristics and mechanical stability have been fully inkjet printed on ultra-flexible polymer films [270]. AM has already enable significant benefits for fabrication of thin film and organic FETs with high resolution [271–273].

3.4.2. *Printed circuit boards*

Fully printed circuit boards (PCBs) can be produced using inkjet printing of the conductive traces, offering highly customisable and low-waste manufacturing. Several companies such as Elephantech and PV Nanocell (see Table 2), have already adopted inkjet processes for PCB fabrication. Recently, highly flexible PCBs were printed on a stretched PDMS substrate to induce wrinkles in the Ag traces when the strain is released [274] and demonstrated spiral conductive tracks manufactured by MM-IJ3DP (reproduced from Ref. [87]) (Fig. 8c). The next step is to enable multi-layer printing for greater circuit density. BotFactory (Table 2) achieved this by coating each layer of circuitry with a dielectric mixture of UV-curable acrylates and urethanes, allowing gaps for vias to join up to 4 layers together. A catalyst-based approach was used to form two-sided PCBs on a paper substrate, including printed vias [275]. Here, silver nanoparticles were inkjet-printed as catalysts for electroless copper deposition, with the depth of metallisation optimised by the amount of deposited ink. Alternatively, vias were printed only using Ag nanoparticle ink, however, circuit failure occurred when the PCB was folded due to the poor adhesion [276].

Recently, Nano Dimension achieved accurate deposition of silver at desired places within its build volume, with the dielectric acting as a support matrix and an electrical insulator. Although limited to a 3 mm build height, this is sufficient to print native componentry, such as inductors or antennas, within the multi-layered PCB [257]. Free-standing and encapsulated vertical silver interconnects were produced with heights up to 10 mm high and an aspect ratio approaching 50 [261], potentially enabling inkjet printing of space-efficient PCBs [261].

3.4.3. Antennas

Manufacturing of antennas requires flexibility of deposition to produce the geometries needed for designed bandwidth, gain, and directionality [277]. Several two-dimensional antennas have been inkjet-printed using Ag NP inks and graphene-based inks [278,279]. More recently, 3D deposition was demonstrated by the PolyJet system from Stratasys, where selective UV-curing of polymer precursor inks enabled the inkjet-printing of complex 3-dimensional polymeric structures [280], which can be can be functionalised by conformal printing onto them. A printed two-turn helix attached to a Fresnel lens was functionalised with inkjet-printed silver NPs onto the outer edge of the helix [281], resulting in a fully inkjet-printed, 3-dimensional antenna, with the lens providing 4.6 dB of gain.

Exploiting flexible electronics can also give pseudo-three-dimensional printing by printing on a substrate in the shape of a cube's net and then folding it up to give a three-dimensional shape for improved antenna design as well as space to fit internal electronics. Kimionis et al. [282] inkjet-printed silver patches on a polymer substrate, which was first printed separately with the PolyJet system. The fold-lines were made from a shape-memory polymer capable of self-assembling and subtly changing shape under temperature fluctuations. The antenna had characteristics modified by its shape, so – combined with some electronics packed into the internal void to harness RF energy through the antenna – it could act as a wireless temperature sensor, potentially as part of a large network. In other reports, the assembly of multiple functional components within one structure are demonstrated (Fig. 8a). Origami-like antennae printed on paper, after folding and sealing, were shown to float and be waterproof. Other examples combine antennae, sensors, PCBs and air capacitors. While a few examples have emerged in the literature, there is still a significant need for the development of truly 3D inkjet-printed architectures to realise complete 3D inkjet-printed electronics.

3.4.4. Multi-material inkjet 3D printing (MM-IJ3DP) for 3D electronics

Although there has been significant progress in fully printed electronics, such as multi-material heterostructures or planar structures, printing does not offer the voxel-wise control which will enable 3D integrated electronics. Further developments are constantly required to enable the manufacture of 3D electronics, due to the complexity of the circuits in 3D and the need for the assembly of different components. Therefore, there is a strong interest in voxel-wise multi-material inkjet 3D printing for 3D electronics. Multi-material inkjet-based 3D printing (MM-IJ3DP) integrates multiple DOD printheads within one machine, which enables the co-printing of different materials at a pico-litre scale (Fig. 8d), offering a voxel-control, unlike its 2D counterpart.

There are several challenges facing the fabrication of 3D electronics through MM-IJ3DP. Different inks require different energy sources to either functionalise or cure them, such as infrared (IR) or ultraviolet (UV) light for solidification (Fig. 8d), or intense pulsed light (IPL) for sintering [51,52]. In the solidification process, the entire structure is exposed, and sample damage could occur and should be considered in the formulating process. For example, to sinter metallic nanoparticle inks, elevated temperatures (120–150 °C) are required [53], which can be detrimental to polymeric substrates underneath [54]. To date, this challenge is addressed by optimizing ink formulations and the solidification process [40]. For example, inkjet-printable polyimide was reported which was thermally stable up to 400 °C [55] and UV light was used to replace the thermal sintering of silver nanoparticles in dielectric polymeric materials [56]. The interface in MM-IJ3DP between different materials is another crucial factor that should be considered when formulating the inks [26]. The preferable scenario is an interface, where the two distinct materials either inter-diffuse into each other in a controlled way or have a covalent bonding, preventing delamination or early failure [6].

4. Concluding remarks and outlook

Inkjet printing is an important AM technique in the field of electronics due to a number of appealing advantages, such as a high degree of fabrication flexibility and the possibility to use various functional inks. Electronic devices including but not limited to sensors, transistors, capacitors, displays, PCBs, solar cells, and batteries have been successfully developed via inkjet printing. The functional inks for inkjet printing can be broadly categorized as conductive polymer inks, low dimensional inks, and composite inks. This review has comprehensively highlighted a wide range of functional inks and their formulation strategies, the inkjet printing process for both single-material and multi-material inks, and inkjet-printed electronic devices within the current state-of-the-art.

Inkjet printing has been extensively used to create 2D planar electronic devices. Recently, increasing attention is focused on manufacturing of fully inkjet-printed 3D integrated electronic devices [267–269]. 2D planar printing is faster compared to 3D printing and allows for rapid prototyping applications. This means that the functionality of the deposited materials can be studied before they are used in 3D devices. It is important to note that 3D printed integrated electronic devices are not created directly from 3D CAD data, however, recent development in multi-material AM technologies and growing availability of functional materials could offer opportunities for fully 3D printed electronics.

Although an increasing number of articles reports the fabrication of fully inkjet-printed electronics, taking advantage of the technique in terms of the scalability, the adaptable digital device design, and the low-waste additive nature of the manufacture, a particular lack of free-standing, 3D inkjet-printed devices is notable. Several works discussed above rely on use of supporting substrate, with devices deposited on top in the form of 2D circuits. However, as reported in recent studies, the integrated 3D electronics employs printed layer as a substrate for the formation of heterostructures or 3D electronic configurations [267–269]. Saleh et al. [87] report circuitry deposited within 3D polymeric structures using a single MJ system, with Ag NP and TPGDA inks jetted in the same process via a piezo-based inkjet system and cured in real-time with a UV light source. This is a promising approach to the realisation of 3D printed objects with embedded electronic functionalities, yet each of the inks is jetted separately from individual cartridges. Additional challenges in realisation of 3D electronics are process-related, where the micro-scale resolution of the deposited structure presents obstacles for fabrication of miniaturised devices. This requires further technological advancements of the hardware as well as understanding of and optimization of the printing strategies. Also, the need for post-processing to achieve the function can bring undesirable complexity to the manufacturing process.

A potential future direction within inkjet-printed electronic applications should focus on the inclusion of electronically active fillers into structurally supportive (polymeric) matrices for 3D printed devices fabricated entirely through MMIJ3DP and cured in real-time. Such an approach exploits both the multifunctionality of the ink materials and the multifunctional MMIJ3DP process. This will require optimisation of the filler content to find a balance between the final electronic properties and the initial jettability of the ink, where a higher solid loading typically leads to increased percolation pathways or improved performance yet challenges the viscosity limitations of the inkjet printing process. Furthermore, the effect of filler content on composite curability must be addressed, notably in the case of light-based post-processing methods, where excessive fillers may obscure light penetration and hinder effective curing. Saleh et al. [15] combined magnetic iron oxide with a UV-curable resin, demonstrating successful material jetting and real-time curing of 3D structures, along with their electromagnetic characterisation. Likewise, functional inks incorporating 0D, 1D and 2D fillers with a wide variety of electronic properties, should be developed and deposited in different combinations via MMIJ3DP for future

demonstrations of fully inkjet-printed 3D devices that can be deposited and post-processed in a scalable manner. Furthermore, future research and development should also be focused on improving the printed resolution, low sensitivity of printed devices, and limited range towards fully 3D printed functional devices.

Although there are several challenges for MM-IJ3DP as a production tool for electronics, we are also seeing a growing interest as well as impressive studies that are targeting these challenges. Predictive modelling has been introduced as a solution to help the user predict whether a failure could happen with a chosen combination of materials as well as whether the chosen set of solidification processes will lead to sample cracking or delamination by residual stresses or thermal expansion. Tim et al. [283] presented a finite element analysis method to analyse and predict product quality using acrylic and silver nanoparticles as an example of multi-material inkjet-printed electronics. Professor Bailey from the University of Greenwich introduced an indicative manufacturing process where an artificial intelligence (AI) monitoring unit was introduced to help improve the quality of manufactured products [283]. Inkbit3D also presented their latest machine vision and AI technology that allows the machine to in-line monitor parts shrinkage and distortions, provide feedback to the machine and compensate for these variations. All these modelling and in-line monitoring technologies can largely improve the manufacturing accuracy and production yield for MM-IJ3DP for printed electronics [283].

The inkjet technology still has a way to go in some areas. A better resolution will be needed to break into the microdevices market in a major way, and some materials are unavailable to print, whilst others still fall behind in performance compared to other production processes. The largest obstacle is still the limitations of going into the third dimension, although work from academia and industry alike are certainly looking to break through soon, be it vertical interconnects, high-density PCBs, or folded structures.

Declaration of Competing Interest

The author(s) declared no potential conflicts of interest with respect to the research, authorship, and/or publication of this article.

Data availability

No data was used for the research described in the article.

Acknowledgements

This work was funded by the Engineering and Physical Sciences Research Council Programme Grant [grant number EP/P031684/1].

References

[1] S.A.M. Tofail, E.P. Koumoulos, A. Bandyopadhyay, S. Bose, L. O'Donoghue, C. Charitidis, Mater. Today 21 (2018) 22–37.
[2] J.Y. Lee, J. An, C.K. Chua, Appl. Mater. Today 7 (2017) 120–133.
[3] X. Zheng, H. Lee, T.H. Weisgraber, M. Shusteff, J. DeOtte, E.B. Duoss, J.D. Kuntz, M.M. Biener, Q. Ge, J.A. Jackson, Science (80-.) 344 (2014) 1373–1377.
[4] Y.W.D. Tay, B. Panda, S.C. Paul, N.A. Noor Mohamed, M.J. Tan, K.F. Leong, Virtual Phys. Prototyp. 12 (2017) 261–276.
[5] A. Uriondo, M. Esperon-Miguez, S. Perinpanayagam, Proc. Inst. Mech. Eng. Part G J. Aerosp. Eng. 229 (2015) 2132–2147.
[6] Y. He, R. Foralosso, G.F. Trindade, A. Ilchev, L. Ruiz-Cantu, E.A. Clark, S. Khaled, R.J.M. Hague, C.J. Tuck, F.R.A.J. Rose, Adv. Ther. 3 (2020), 1900187.
[7] T. Ahmadraji, L. Gonzalez-Macia, T. Ritvonen, A. Willert, S. Ylimaula, D. Donaghy, S. Tuurala, M. Suhonen, D. Smart, A. Morrin, V. Efremov, R. R. Baumann, M. Raja, A. Kemppainen, A.J. Killard, Anal. Chem. 89 (2017) 7447–7454.
[8] A. Kamyshny, S. Magdassi, Chem. Soc. Rev. 48 (2019) 1712–1740.
[9] L. Yang, H. Hu, A. Scholz, F. Feist, G. Cadilha Marques, S. Kraus, N. M. Bojanowski, E. Blasco, C. Barner-Kowollik, J. Aghassi-Hagmann, M. Wegener, Nat. Commun. 14 (2023) 1103.
[10] A. Willert, F.Z. Tabary, T. Zubkova, P.E. Santangelo, M. Romagnoli, R. R. Baumann, Int. J. Hydrogen Energy 47 (2022) 20973–20986.
[11] Y. Khan, A. Thielens, S. Muin, J. Ting, C. Baumbauer, A.C. Arias, Adv. Mater. 32 (2020), 1905279.
[12] H. Lee, C. Bae, L.T. Duy, I. Sohn, D. Kim, Y. Song, Y. Kim, N. Lee, Adv. Mater. 28 (2016) 3069–3077.
[13] S. Faraji, F.N. Ani, Renew. Sustain. Energy Rev. 42 (2015) 823–834.
[14] C. Chen, H. Kang, S. Hsiao, P. Yang, K. Chiang, H. Lin, Adv. Mater. 26 (2014) 6647–6652.
[15] E. Saleh, P. Woolliams, B. Clarke, A. Gregory, S. Greedy, C. Smartt, R. Wildman, I. Ashcroft, R. Hague, P. Dickens, C. Tuck, Addit. Manuf. 13 (2017) 143–148.
[16] Y. He, B. Begines, G.F. Trindade, M. Abdi, J.F. Dubern, E. Prina, A.L. Hook, G. Choong, J. Ledesma, C.J. Tuck, F.R.A.J. Rose, R. Hague, C.J. Roberts, D. de Focatiis, I.A. Ashcroft, P. Williams, D.J. Irvine, M.R. Alexander, R.D. Wildman, ChemRxiv (2020).
[17] J. Lemarchand, N. Bridonneau, N. Battaglini, F. Carn, G. Mattana, B. Piro, S. Zrig, V. Noël, Angew. Chemie Int. Ed. 61 (2022), e202200166.
[18] D.F. Fernandes, C. Majidi, M. Tavakoli, J. Mater. Chem. C 7 (2019) 14035–14068.
[19] B. Derby, Annu. Rev. Mater. Res. 40 (2010) 395–414.
[20] A. Sajedi-Moghaddam, E. Rahmanian, N. Naseri, ACS Appl. Mater. Interfaces 12 (2020) 34487–34504.
[21] B. Derby, N. Reis, MRS Bull. 28 (2003) 815–818.
[22] G. Rivers, J.S. Austin, Y. He, A. Thompson, N. Gilani, N. Roberts, P. Zhao, C. J. Tuck, R.J.M. Hague, R.D. Wildman, L. Turyanska, Addit. Manuf. 66 (2023), 103452.
[23] B. Weng, R. Shepherd, J. Chen, G.G. Wallace, J. Mater. Chem. 21 (2011) 1918–1924.
[24] N.T. Brannelly, A.J. Killard, Electroanalysis 29 (2017) 162–171.
[25] E. Bihar, D. Corzo, T.C. Hidalgo, D. Rosas-Villalva, K.N. Salama, S. Inal, D. Baran, Adv. Mater. Technol. 5 (2020), 2000226.
[26] B. Wang, L. Kari, Polym. 13 (2021).
[27] G.F. Trindade, F. Wang, J. Im, Y. He, A. Balogh, D. Scurr, I. Gilmore, M. Tiddia, E. Saleh, D. Pervan, L. Turyanska, C.J. Tuck, R. Wildman, R. Hague, C.J. Roberts, Commun. Mater. 2 (2021) 47.
[28] J. Im, G.F. Trindade, T.T. Quach, A. Sohaib, F. Wang, J. Austin, L. Turyanska, C. J. Roberts, R. Wildman, R. Hague, C. Tuck, A.C.S. Appl, Nano Mater. 5 (2022) 6708–6716.
[29] M.S. Rager, T. Aytug, G.M. Veith, P. Joshi, ACS Appl. Mater. Interfaces 8 (2016) 2441–2448.
[30] V. Beedasy, P.J. Smith, Materials (Basel) 13 (2020) 704.
[31] D. McManus, S. Vranic, F. Withers, V. Sanchez-Romaguera, M. Macucci, H. Yang, R. Sorrentino, K. Parvez, S.K. Son, G. Iannaccone, K. Kostarelos, G. Fiori, C. Casiraghi, Nat. Nanotechnol. 12 (2017) 343–350.
[32] J.S. Austin, N.D. Cottam, C. Zhang, F. Wang, J.H. Gosling, O. Nelson-Dummet, T. S.S. James, P.H. Beton, G.F. Trindade, Y. Zhou, Nanoscale 15 (2023) 2134–2142.
[33] O. Song, D. Rhee, J. Kim, Y. Jeon, V. Mazánek, A. Söll, Y.A. Kwon, J.H. Cho, Y. H. Kim, Z. Sofer, J. Kang, NPJ 2D Mater. Appl. 6 (2022) 64.
[34] S. Chung, K. Cho, T. Lee, Adv. Sci. 6 (2019), 1801445.
[35] L. Nayak, S. Mohanty, S.K. Nayak, A. Ramadoss, J. Mater. Chem. C 7 (2019) 8771–8795.
[36] K. Yan, J. Li, L. Pan, Y. Shi, APL Mater. 8 (2020), 120705.
[37] G.L. Goh, H. Zhang, T.H. Chong, W.Y. Yeong, Adv. Electron. Mater. 7 (2021), 2100445.
[38] Z. Zhou, L.Ruiz Cantu, X. Chen, M.R. Alexander, C.J. Roberts, R. Hague, C. Tuck, D. Irvine, R. Wildman, Addit. Manuf. 29 (2019), 100792.
[39] R. Noguera, M. Lejeune, T. Chartier, J. Eur. Ceram. Soc. 25 (2005) 2055–2059.
[40] P. He, B. Derby, Adv. Mater. Interfaces 4 (2017), 1700944.
[41] F. Torrisi, T. Hasan, W. Wu, Z. Sun, A. Lombardo, T.S. Kulmala, G.W. Hsieh, S. Jung, F. Bonaccorso, P.J. Paul, ACS Nano 6 (2012) 2992–3006.
[42] O.S. Kwon, H. Kim, H. Ko, J. Lee, B. Lee, C.H. Jung, J.H. Choi, K. Shin, Carbon N. Y. 58 (2013) 116–127.
[43] F. Scuratti, J.M. Salazar-Rios, A. Luzio, S. Kowalski, S. Allard, S. Jung, U. Scherf, M.A. Loi, M. Caironi, Adv. Funct. Mater. 31 (2021), 2006895.
[44] I.J. Fernandes, A.F. Aroche, A. Schuck, P. Lamberty, C.R. Peter, W. Hasenkamp, T. Rocha, Sci. Rep. 10 (2020) 8878.
[45] C.A. Lamont, T.M. Eggenhuisen, M.J.J. Coenen, T.W.L. Slaats, R. Andriessen, P. Groen, Org. Electron. 17 (2015) 107–114.
[46] A. Matavz, R.C. Frunza, A. Drnovsek, V. Bobnar, B. Malic, J. Mater. Chem. C 4 (2016) 5634–5641.
[47] S. Jeong, H.C. Song, W.W. Lee, S.S. Lee, Y. Choi, W. Son, E.D. Kim, C.H. Paik, S. H. Oh, B.H. Ryu, Langmuir 27 (2011) 3144–3149.
[48] P. Yang, L. Zhang, dong J. Kang, R. Strahl, T. Kraus, Adv. Opt. Mater. 8 (2020), 1901429.
[49] Y.S. Goo, Y.I. Lee, N. Kim, K.J. Lee, B. Yoo, S.J. Hong, J.D. Kim, Y.H. Choa, Surf. Coatings Technol. 205 (2010) S369–S372.
[50] S.H. Lee, Y.J. Cho, J. Electr. Eng. Technol. 7 (2012) 91–96.
[51] B.K. Lok, X. Hu, in: 2010 12th Electron. Packag. Technol. Conf., IEEE, 2010, pp. 240–245.
[52] P. Wilson, C. Lekakou, J. Watts, in: 2012 12th IEEE Int. Conf. Nanotechnol, IEEE, 2012, pp. 1–6.
[53] A. Kamyshny, M. Ben-Moshe, S. Aviezer, S. Magdassi, Macromol. Rapid Commun. 26 (2005) 281–288.
[54] J.H. Kim, S. Il Ahn, J.H. Kim, W.C. Zin, Langmuir 23 (2007) 6163–6169.
[55] R.D. Deegan, O. Bakajin, T.F. Dupont, G. Huber, S.R. Nagel, T.A. Witten, Nature 389 (1997) 827–829.
[56] H. Hu, R.G. Larson, J. Phys. Chem. B 110 (2006) 7090–7094.
[57] K.Y. Shin, S.H. Lee, J.H. Oh, J. Micromech. Microeng. 21 (2011) 45012.
[58] Z. Xiong, C. Liu, in: 18th Eur. Microelectron. Packag. Conf., IEEE, 2011, pp. 1–4.

[59] J. Park, J. Moon, Langmuir 22 (2006) 3506–3513.
[60] D. Kim, S. Jeong, B.K. Park, J. Moon, Appl. Phys. Lett. 89 (2006), 264101.
[61] W.D. Ristenpart, P.G. Kim, C. Domingues, J. Wan, H.A. Stone, Phys. Rev. Lett. 99 (2007), 234502.
[62] M. Kuang, J. Wang, B. Bao, F. Li, L. Wang, L. Jiang, Y. Song, Adv. Opt. Mater. 2 (2013) 34–38.
[63] G. Hu, L. Yang, Z. Yang, Y. Wang, X. Jin, J. Dai, Q. Wu, S. Liu, X. Zhu, X. Wang, T. C. Wu, R.C.T. Howe, T. Albrow-Owen, L.W.T. Ng, Q. Yang, L.G. Occhipinti, R. I. Woodward, E.J.R. Kelleher, Z. Sun, X. Huang, M. Zhang, C.D. Bain, T. Hasan, Sci. Adv. 6 (2020) eaba5029.
[64] S. Abdolhosseinzadeh, X. Jiang, H. Zhang, J. Qiu, C.(John) Zhang, Mater. Today (2021).
[65] H. Liu, W. Xu, W. Tan, X. Zhu, J. Wang, J. Peng, Y. Cao, J. Colloid Interface Sci. 465 (2016) 106–111.
[66] C. Sturgess, C.J. Tuck, I.A. Ashcroft, R.D. Wildman, J. Mater. Chem. C 5 (2017) 9733–9745.
[67] I. Louzao, B. Koch, V. Taresco, L. Ruiz-Cantu, D.J. Irvine, C.J. Roberts, C. Tuck, C. Alexander, R. Hague, R. Wildman, M.R. Alexander, ACS Appl. Mater. Interfaces 10 (2018) 6841–6848.
[68] T. Beduk, E. Bihar, S.G. Surya, A.N. Castillo, S. Inal, K.N. Salama, Sensors Actuators B Chem. 306 (2020), 127539.
[69] M.N. Gueye, A. Carella, N. Massonnet, E. Yvenou, S. Brenet, J. Faure-Vincent, S. Pouget, F. Rieutord, H. Okuno, A. Benayad, R. Demadrille, J.P. Simonato, Chem. Mater. 28 (2016) 3462–3468.
[70] Y.H. Kim, C. Sachse, M.L. MacHala, C. May, L. Müller-Meskamp, K. Leo, Adv. Funct. Mater. 21 (2011) 1076–1081.
[71] M.N. Gueye, A. Carella, J. Faure-Vincent, R. Demadrille, J.P. Simonato, Prog. Mater. Sci. 108 (2020), 100616.
[72] R. Balint, N.J. Cassidy, S.H. Cartmell, Acta Biomater. 10 (2014) 2341–2353.
[73] X. Li, Z. Liu, Z. Zhou, H. Gao, G. Liang, D. Rauber, C.W.M. Kay, P. Zhang, A.C. S. Appl, Polym. Mater. 2021 (2020) 98–103.
[74] T. Rödlmeier, T. Marszalek, M. Held, S. Beck, C. Müller, R. Eckstein, A.J. Morfa, R. Lovrincic, A. Pucci, U. Lemmer, J. Zaumseil, W. Pisula, G. Hernandez-Sosa, Chem. Mater. 29 (2017) 10150–10158.
[75] R. Kroon, D.A. Mengistie, D. Kiefer, J. Hynynen, J.D. Ryan, L. Yu, C. Müller, Chem. Soc. Rev. 45 (2016) 6147–6164.
[76] A. Giuri, S. Masi, A. Listorti, G. Gigli, S. Colella, C. Esposito Corcione, A. Rizzo, Nano Energy 54 (2018) 400–408.
[77] H. Yuk, B. Lu, S. Lin, K. Qu, J. Xu, J. Luo, X. Zhao, Nat. Commun. 11 (2020) 1–8.
[78] A. Giuri, E. Saleh, A. Listorti, S. Colella, A. Rizzo, C. Tuck, C.Esposito Corcione, Nanomaterials 9 (2019) 582.
[79] A. De Girolamo Del Mauro, R. Diana, I.A. Grimaldi, F. Loffredo, P. Morvillo, F. Villani, C. Minarini, Polym. Compos. 34 (2013) 1493–1499.
[80] B. Fan, X. Mei, J. Ouyang, Macromolecules 41 (2008) 5971–5973.
[81] H. Ling, R. Chen, Q. Huang, F. Shen, Y. Wang, X. Wang, Green Chem. 22 (2020) 3208–3215.
[82] Y. Wang, C. Zhu, R. Pfattner, H. Yan, L. Jin, S. Chen, F. Molina-Lopez, F. Lissel, J. Liu, N.I. Rabiah, Z. Chen, J.W. Chung, C. Linder, M.F. Toney, B. Murmann, Z. Bao, Sci. Adv. (2017) 3.
[83] M.Y. Teo, N. Ravichandran, N. Kim, S. Kee, L. Stuart, K.C. Aw, J. Stringer, ACS Appl. Mater. Interfaces 11 (2019) 37069–37076.
[84] X. Fan, W. Nie, H. Tsai, N. Wang, H. Huang, Y. Cheng, R. Wen, L. Ma, F. Yan, Y. Xia, Adv. Sci. 6 (2019), 1900813.
[85] B.Y. Ahn, S.B. Walker, S.C. Slimmer, A. Russo, A. Gupta, S. Kranz, E.B. Duoss, T. F. Malkowski, J.A. Lewis, J. Vis. Exp. JoVE (2011).
[86] Q. Huang, W. Shen, Q. Xu, R. Tan, W. Song, Mater. Chem. Phys. 147 (2014) 550–556.
[87] E. Saleh, F. Zhang, Y. He, J. Vaithilingam, J.L. Fernandez, R. Wildman, I. Ashcroft, R. Hague, P. Dickens, C. Tuck, Adv. Mater. Technol. 2 (2017), 1700134.
[88] A. Maattanen, P. Ihalainen, P. Pulkkinen, S. Wang, H. Tenhu, J. Peltonen, ACS Appl. Mater. Interfaces 4 (2012) 955–964.
[89] Y. Khan, F.J. Pavinatto, M.C. Lin, A. Liao, S.L. Swisher, K. Mann, V. Subramanian, M.M. Maharbiz, A.C. Arias, Adv. Funct. Mater. 26 (2016) 1004–1013.
[90] Y. Ren, J. Virkki, L. Sydänheimo, L. Ukkonen, Electron. Lett. 50 (2014) 1504–1505.
[91] B.N. Altay, V.S. Turkani, A. Pekarovicova, P.D. Fleming, M.Z. Atashbar, M. Bolduc, S.G. Cloutier, Sci. Rep. 11 (2021) 1–12.
[92] E. Gracia-Espino, G. Sala, F. Pino, N. Halonen, J. Luomahaara, J. Mäklin, G. Toth, K. Kordás, H. Jantunen, M. Terrones, ACS Nano 4 (2010) 3318–3324.
[93] S. Azoubel, S. Shemesh, S. Magdassi, Nanotechnology 23 (2012), 344003.
[94] Q. He, S.R. Das, N.T. Garland, D. Jing, J.A. Hondred, A.A. Cargill, S. Ding, C. Karunakaran, J.C. Claussen, ACS Appl. Mater. Interfaces 9 (2017) 12719–12727.
[95] J. Li, F. Ye, S. Vaziri, M. Muhammed, M.C. Lemme, M. Östling, Adv. Mater. 25 (2013) 3985–3992.
[96] N. Karim, S. Afroj, A. Malandraki, S. Butterworth, C. Beach, M. Rigout, K. S. Novoselov, A.J. Casson, S.G. Yeates, J. Mater. Chem. C 5 (2017) 11640–11648.
[97] R. Worsley, L. Pimpolari, D. McManus, N. Ge, R. Ionescu, J.A. Wittkopf, A. Alieva, G. Basso, M. MacUcci, G. Iannaccone, K.S. Novoselov, H. Holder, G. Fiori, C. Casiraghi, ACS Nano 13 (2019) 54–60.
[98] M. Baklar, P.H. Wöbkenberg, D. Sparrowe, M. Gonçalves, I. McCulloch, M. Heeney, T. Anthopoulos, N. Stingelin, J. Mater. Chem. 20 (2010) 1927.
[99] Z. Stempien, T. Rybicki, E. Rybicki, M. Kozanecki, M.I. Szynkowska, Synth. Met. 202 (2015) 49–62.
[100] J. Dong, G. Portale, Adv. Mater. Interfaces 7 (2020), 2000641.
[101] T.R. Chou, S.H. Chen, Y. Te Chiang, Y.T. Lin, C.Y. Chao, J. Mater. Chem. C 3 (2015) 3760–3766.
[102] N. Kim, S. Kee, S.H. Lee, B.H. Lee, Y.H. Kahng, Y.R. Jo, B.J. Kim, K. Lee, Adv. Mater. 26 (2014) 2268–2272.
[103] Z. Xiong, C. Liu, Org. Electron. 13 (2012) 1532–1540.
[104] L. Pan, G. Yu, D. Zhai, H.R. Lee, W. Zhao, N. Liu, H. Wang, B.C.K. Tee, Y. Shi, Y. Cui, Z. Bao, Proc. Natl. Acad. Sci. U. S. A. 109 (2012) 9287–9292.
[105] N. Graddage, T.Y. Chu, H. Ding, C. Py, A. Dadvand, Y. Tao, Org. Electron. 29 (2016) 114–119.
[106] Y. He, F. Zhang, E. Saleh, J. Vaithilingam, N. Aboulkhair, B. Begines, C.J. Tuck, R. J.M. Hague, I.A. Ashcroft, R.D. Wildman, Addit. Manuf. 16 (2017) 153–161.
[107] A. Moya, E. Sowade, F.J. del Campo, K.Y. Mitra, E. Ramon, R. Villa, R. R. Baumann, G. Gabriel, Org. Electron. 39 (2016) 168–176.
[108] A. Dadvand, J. Lu, C. Py, T.Y. Chu, R. Movileanu, Y. Tao, Org. Electron. 30 (2016) 213–218.
[109] J. Zhang, A. Chaudhari, H. Wang, J. Manuf. Process. 45 (2019) 710–719.
[110] F. Zhang, E. Saleh, J. Vaithilingam, Y. Li, C.J. Tuck, R.J.M. Hague, R.D. Wildman, Y. He, Addit. Manuf. 25 (2019) 477–484.
[111] B.J. Kang, C.K. Lee, J.H. Oh, Microelectron. Eng. 97 (2012) 251–254.
[112] J. Szczech, C. Megaridis, J. Zhang, D. Gamota, Microscale Thermophys. Eng. 8 (2004) 327–339.
[113] J. Yang, P. He, B. Derby, ACS Appl. Mater. Interfaces 14 (2022) 39601–39609.
[114] J. Vaithilingam, E. Saleh, L. Körner, R.D. Wildman, R.J.M. Hague, R.K. Leach, C. J. Tuck, Mater. Des. 139 (2018) 81–88.
[115] W. Shen, X. Zhang, Q. Huang, Q. Xu, W. Song, Nanoscale 6 (2014) 1622–1628.
[116] H.H. Lee, K.S. Chou, K.C. Huang, Nanotechnology 16 (2005) 2436.
[117] B.T. Anto, S. Sivaramakrishnan, L.L. Chua, P. K.H.Ho, Adv. Funct. Mater. 20 (2010) 296–303.
[118] K.T. Park, Y.S. Cho, I. Jeong, D. Jang, H. Cho, Y. Choi, T. Lee, Y. Ko, J. Choi, S. Y. Hong, M.W. Oh, S. Chung, C.R. Park, H. Kim, Adv. Energy Mater. 12 (2022), 2200256.
[119] Y. Farraj, M. Grouchko, S. Magdassi, Chem. Commun. 51 (2015) 1587–1590.
[120] R. Sliz, M. Lejay, J.Z. Fan, M.J. Choi, S. Kinge, S. Hoogland, T. Fabritius, F. P. García de Arquer, E.H. Sargent, ACS Nano 13 (2019) 11988–11995.
[121] J.H. Yoo, S.G. Jeong, S.H. Choi, S. Bin Kwon, Y.H. Song, D.H. Yoon, Ceram. Int. 47 (2021) 6041–6048.
[122] S. Wang, X. Wu, J. Lu, Z. Luo, H. Xie, X. Zhang, K. Lin, Y. Wang, Nanomaterials 12 (2022) 842.
[123] P. Patil, S. Patil, P. Kate, A.A. Kulkarni, Nanoscale Adv. 3 (2021) 240–248.
[124] W.B. Liu, S. Pei, J. Du, B. Liu, L. Gao, Y. Su, C. Liu, H.M. Cheng, Adv. Funct. Mater. 21 (2011) 2330–2337.
[125] V. Soum, S. Park, A.I. Brilian, Y. Kim, M.Y. Ryu, T. Brazell, F.J. Burpo, K. K. Parker, O.S. Kwon, K. Shin, ACS Omega 4 (2019) 8626–8631.
[126] K. Parvez, R. Worsley, A. Alieva, A. Felten, C. Casiraghi, Carbon N. Y. 149 (2019) 213–221.
[127] J. Ma, S. Zheng, Y. Cao, Y. Zhu, P. Das, H. Wang, Y. Liu, J. Wang, L. Chi, S. (Frank) Liu, Z.S. Wu, Adv. Energy Mater. 11 (2021), 2100746.
[128] E. Marzbanrad, H.H. Khaligh, (2023).
[129] H. Kang, G.H. Lee, H. Jung, J.W. Lee, Y. Nam, ACS Nano 12 (2018) 1128–1138.
[130] S. Halivni, S. Shemesh, N. Waiskopf, Y. Vinetsky, S. Magdassi, U. Banin, Nanoscale 7 (2015) 19193–19200.
[131] K. Saito, K. McGehee, K. Manabe, Y. Norikane, RSC Adv. 11 (2021) 22376–22380.
[132] S.K. Gupta, M.F. Prodanov, W. Zhang, V.V. Vashchenko, T. Dudka, A.L. Rogach, A.K. Srivastava, Nanoscale 11 (2019) 20837–20846.
[133] J. Lin, M. Kilani, G. Mao, Adv. Mater. Technol. (2023), 2202038.
[134] R. Madhavan, J. Mater. Sci. Mater. Electron. 33 (2022) 3465–3484.
[135] D.J. Finn, M. Lotya, G. Cunningham, R.J. Smith, D. McCloskey, J.F. Donegan, J. N. Coleman, J. Mater. Chem. C 2 (2014) 925–932.
[136] Y. Hernandez, V. Nicolosi, M. Lotya, F.M. Blighe, Z. Sun, S. De, I.T. McGovern, B. Holland, M. Byrne, Y.K. Gun'Ko, J.J. Boland, P. Niraj, G. Duesberg, S. Krishnamurthy, R. Goodhue, J. Hutchison, V. Scardaci, A.C. Ferrari, J. N. Coleman, Nat. Nanotechnol. 3 (2008) 563–568.
[137] J.A. Desai, S. Mazumder, R.F. Hossain, A.B. Kaul, J. Vac. Sci. Technol. B Nanotechnol. Microelectron. Mater. Process. Meas. Phenom. 38 (2020) 52201.
[138] E. Brown, P. Yan, H. Tekik, A. Elangovan, J. Wang, D. Lin, J. Li, Mater. Des. 170 (2019), 107689.
[139] B. Dai, L. Fu, L. Liao, N. Liu, K. Yan, Y. Chen, Z. Liu, Nano Res. 4 (2011) 434–439.
[140] P. He, B. Derby, 2D Mater. 4 (2017) 21021.
[141] Y. Gao, W. Shi, W. Wang, Y. Leng, Y. Zhao, Ind. Eng. Chem. Res. 53 (2014) 16777–16784.
[142] K. Arapov, R. Abbel, H. Friedrich, Faraday Discuss 173 (2014) 323–336.
[143] T. Carey, S. Cacovich, G. Divitini, jiesheng Ren, A. Mansouri, J.M. Kim, C. Wang, C. Ducati, R. Sordan, F. Torrisi, Nat. Commun. 8 (2017) 1202.
[144] K. Liang, R. Wang, H. Ren, D. Li, Y. Tang, Y. Wang, Y. Chen, C. Song, F. Li, G. Liu, H. Wang, W.R. Leow, B. Zhu, Adv. Opt. Mater. 10 (2022), 2201754.
[145] J. Li, M.M. Naiini, S. Vaziri, M.C. Lemme, M. Östling, Adv. Funct. Mater. 24 (2014) 6524–6531.
[146] A.G. Kelly, T. Hallam, C. Backes, A. Harvey, A.S. Esmaeily, I. Godwin, J. Coelho, V. Nicolosi, J. Lauth, A. Kulkarni, S. Kinge, L.D.A. Siebbeles, G.S. Duesberg, J. N. Coleman, Science (80-.) 356 (2017) 69–73.
[147] C.W. Wu, B. Unnikrishnan, I.W.P. Chen, S.G. Harroun, H.T. Chang, C.C. Huang, Energy Storage Mater. 25 (2020) 563–571.
[148] H. Abdolmaleki, A.B. Haugen, K.B. Buhl, K. Daasbjerg, S. Agarwala, Adv. Sci. 10 (2023), 2205942.
[149] E. Saleh, 3D 4D Print, Polym. Nanocomposite Mater. (2020) 505–525.

[150] W. Zhang, E. Bi, M. Li, L. Gao, Colloids Surfaces A Physicochem. Eng. Asp. 490 (2016) 232–240.
[151] L. Li, M. Gao, Y. Guo, J. Sun, Y. Li, F. Li, Y. Song, Y. Li, J. Mater. Chem. C 5 (2017) 2800–2806.
[152] J. Zhao, M. Song, C. Wen, S. Majee, D. Yang, B. Wu, S.L. Zhang, Z.B. Zhang, J. Micromech. Microeng. 28 (2018).
[153] J. Brenneman, D.Z. Tansel, G.K. Fedder, R. Panat, Extrem. Mech. Lett. 43 (2021).
[154] K.D. Harris, A.L. Elias, H.J. Chung, J. Mater. Sci. (2015) 2771–2805.
[155] D. Zhai, T. Zhang, J. Guo, X. Fang, J. Wei, Colloids Surfaces A Physicochem, Eng. Asp. 424 (2013) 1–9.
[156] D.J. Kang, Y. Juttke, L. Gonzalez-Garcia, A. Escudero, M. Haft, T. Kraus, Small 16 (2020), e2000928.
[157] K. Kim, M. Jung, B. Kim, J. Kim, K. Shin, O.S. Kwon, S. Jeon, Nano Energy 41 (2017) 301–307.
[158] K.N. Al-Milaji, Q. Huang, Z. Li, T.N. Ng, H. Zhao, ACS Appl. Electron. Mater. 2 (2020) 3289–3298.
[159] Q. Huang, K.N. Al-Milaji, H. Zhao, A.C.S. Appl, Nano Mater. 1 (2018) 4528–4536.
[160] S. Hong, J. Lee, K. Do, M. Lee, J.H. Kim, S. Lee, D.H. Kim, Adv. Funct. Mater. (2017) 27.
[161] P. Sundriyal, S. Bhattacharya, A.C.S. Appl, Energy Mater. 2 (2019) 1876–1890.
[162] Y. Wang, M. Yao, R. Ma, Q. Yuan, D. Yang, B. Cui, C. Ma, M. Liu, D. Hu, J. Mater. Chem. A 8 (2020) 884–917.
[163] M. Mikolajek, T. Reinheimer, N. Bohn, C. Kohler, M.J. Hoffmann, J.R. Binder, Sci. Rep. 9 (2019).
[164] T. Reinheimer, R. Azmi, J.R. Binder, ACS Appl. Mater. Interfaces 12 (2020) 2974–2982.
[165] H. Abdolmaleki, S. Agarwala, Polym. 12 (2020).
[166] G. Zapsas, Y. Patil, Y. Gnanou, B. Ameduri, N. Hadjichristidis, Prog. Polym. Sci. 104 (2020).
[167] F. Torres-Canas, J. Yuan, I. Ly, W. Neri, A. Colin, P. Poulin, Adv. Funct. Mater. 29 (2019).
[168] J. Lim, H. Jung, C. Baek, G.T. Hwang, J. Ryu, D. Yoon, J. Yoo, K.I. Park, J.H. Kim, Nano Energy 41 (2017) 337–343.
[169] H. Xu, X. Hu, H. Yang, Y. Sun, C. Hu, Y. Huang, Adv. Energy Mater. 5 (2015), 1401882.
[170] Y. Lin, J. Chen, M.M. Tavakoli, Y. Gao, Y. Zhu, D. Zhang, M. Kam, Z. He, Z. Fan, Adv. Mater. 31 (2019), e1804285.
[171] S. Wang, N. Liu, J. Tao, C. Yang, W. Liu, Y. Shi, Y. Wang, J. Su, L. Li, Y. Gao, J. Mater. Chem. A 3 (2015) 2407–2413.
[172] B. Li, N. Hu, Y. Su, Z. Yang, F. Shao, G. Li, C. Zhang, Y. Zhang, ACS Appl. Mater. Interfaces 11 (2019) 46044–46053.
[173] J. Diao, J. Yuan, A. Ding, J. Zheng, Z. Lu, Macromol. Mater. Eng. (2018) 303.
[174] K. Chi, Z. Zhang, J. Xi, Y. Huang, F. Xiao, S. Wang, Y. Liu, ACS Appl. Mater. Interfaces 6 (2014) 16312–16319.
[175] N. Li, Y. Jiang, Y. Xiao, B. Meng, C. Xing, H. Zhang, Z. Peng, Nanoscale 11 (2019) 21522–21531.
[176] X.F. Jin, C.R.L. Liu, L. Chen, Y. Zhang, X.J. Zhang, Y.M. Chen, J.J. Chen, Sensors Actuators A Phys. 316 (2020).
[177] J. George, A. Abdelghani, P. Bahoumina, O. Tantot, D. Baillargeat, K. Frigui, S. Bila, H. Hallil, C. Dejous, Sensors (Basel) (2019) 19.
[178] A.S. Alshammari, M.R. Alenezi, K.T. Lai, S.R.P. Silva, Mater. Lett. 189 (2017) 299–302.
[179] M.M. Kiaee, T. Maeder, J. Brugger, Adv. Mater. Technol. 6 (2020).
[180] C.J. Bright, E.C. Nallon, M.P. Polcha, V.P. Schnee, Anal. Chem. 87 (2015) 12270–12275.
[181] Y.Z.N. Htwe, I.N. Hidayah, M. Mariatti, J. Mater. Sci. Mater. Electron. 31 (2020) 15361–15371.
[182] G. Hassan, M.U. Khan, J. Bae, A. Shuja, Sci. Rep. 10 (2020) 18234.
[183] G. Hassan, J. Bae, A. Hassan, S. Ali, C.H. Lee, Y. Choi, Compos. Part A Appl. Sci. Manuf. 107 (2018) 519–528.
[184] H. Minemawari, T. Yamada, H. Matsui, J. Tsutsumi, S. Haas, R. Chiba, R. Kumai, T. Hasegawa, Nature 475 (2011) 364–367.
[185] G. Mattana, A. Loi, M. Woytasik, M. Barbaro, V. Noël, B. Piro, Adv. Mater. Technol. 2 (2017), 1700063.
[186] X. Qiu, X. Gong, X. Zhang, W. Zheng, Coatings 12 (2022) 1893.
[187] C. Wei, W. Su, J. Li, B. Xu, Q. Shan, Y. Wu, F. Zhang, M. Luo, H. Xiang, Z. Cui, Adv. Mater. 34 (2022), 2107798.
[188] L. Liu, Y. Pei, S. Ma, X. Sun, T.J. Singler, Adv. Eng. Mater. 22 (2020), 1901351.
[189] C. Buga, J.C. Viana, Flex. Print. Electron. 7 (2022) 45004.
[190] H.M. Haverinen, R.A. Myllylä, G.E. Jabbour, Appl. Phys. Lett. 94 (2009).
[191] J. Sun, Y. Li, G. Liu, S. Chen, Y. Zhang, C. Chen, F. Chu, Y. Song, ACS Appl. Mater. Interfaces 12 (2020) 22108–22114.
[192] Nano Dimens. Https://Www.Nano-Di.Com/Ame-Dragonfly-Ldm (2021).
[193] T.T.T. Can, T.C. Nguyen, W.S. Choi, Sci. Rep. 9 (2019) 9180.
[194] J. Im, Y. Liu, Q. Hu, G.F. Trindade, C. Parmenter, M. Fay, Y. He, D.J. Irvine, C. Tuck, R.D. Wildman, Adv. Funct. Mater. (2023), 2211920.
[195] F. Mathies, E.J.W. List-Kratochvil, E.L. Unger, Energy Technol. 8 (2020).
[196] D. Dodoo-Arhin, R.C.T. Howe, G. Hu, Y. Zhang, P. Hiralal, A. Bello, G. Amaratunga, T. Hasan, Carbon N. Y. 105 (2016) 33–41.
[197] X. Pi, L. Zhang, D. Yang, J. Phys. Chem. C 116 (2012) 21240–21243.
[198] M.A. Green, Y. Hishikawa, W. Warta, E.D. Dunlop, D.H. Levi, J. Hohl-Ebinger, A. W.H. Ho-Baillie, Prog. Photovoltaics Res. Appl. (2017) 25.
[199] F. Mathies, T. Abzieher, A. Hochstuhl, K. Glaser, A. Colsmann, U.W. Paetzold, G. Hernandez-Sosa, U. Lemmer, A. Quintilla, J. Mater. Chem. A 4 (2016) 19207–19213.
[200] F. Mathies, H. Eggers, B.S. Richards, G. Hernandez-Sosa, U. Lemmer, U. W. Paetzold, ACS Appl. Energy Mater. 1 (2018) 1834–1839.
[201] T.M. Eggenhuisen, Y. Galagan, A.F.K.V. Biezemans, T.M.W.L. Slaats, W. P. Voorthuijzen, S. Kommeren, S. Shanmugam, J.P. Teunissen, A. Hadipour, W.J. H. Verhees, S.C. Veenstra, M.J.J. Coenen, J. Gilot, R. Andriessen, W.A. Groen, J. Mater. Chem. A 3 (2015) 7255–7262.
[202] J. Liu, B. Shabbir, C. Wang, T. Wan, Q. Ou, P. Yu, A. Tadich, X. Jiao, D. Chu, D. Qi, D. Li, R. Kan, Y. Huang, Y. Dong, J. Jasieniak, Y. Zhang, Q. Bao, Adv. Mater. (2019) 31.
[203] L. Zhou, L. Yang, M. Yu, Y. Jiang, C.F. Liu, W.Y. Lai, W. Huang, ACS Appl. Mater. Interfaces 9 (2017) 40533–40540.
[204] F. Hermerschmidt, F. Mathies, V.R.F. Schröder, C. Rehermann, N.Z. Morales, E. L. Unger, E.J.W. List-Kratochvil, Mater. Horizons 7 (2020) 1773–1781.
[205] G. Hu, T. Albrow-Owen, X. Jin, A. Ali, Y. Hu, R.C.T. Howe, K. Shehzad, Z. Yang, X. Zhu, R.I. Woodward, T.C. Wu, H. Jussila, J. Bin Wu, P. Peng, P.H. Tan, Z. Sun, E.J.R. Kelleher, M. Zhang, Y. Xu, T. Hasan, Nat. Commun. 8 (2017).
[206] S.J. Ho, H.C. Hsu, C.W. Yeh, H.S. Chen, ACS Appl. Mater. Interfaces 12 (2020) 33346–33351.
[207] Y. Liu, F. Li, Z. Xu, C. Zheng, T. Guo, X. Xie, L. Qian, D. Fu, X. Yan, ACS Appl. Mater. Interfaces 9 (2017) 25506–25512.
[208] Z. Zhang, T. Si, Sensors Actuators A Phys. 264 (2017) 188–194.
[209] C. Casiraghi, M. Macucci, K. Parvez, R. Worsley, Y. Shin, F. Bronte, C. Borri, M. Paggi, G. Fiori, Carbon N. Y. 129 (2018) 462–467.
[210] Z. Zheng, N. Kim, W.S. Wong, J.T.W. Yeow, Sensors Actuators B Chem. 327 (2021), 128920.
[211] S. Sollami Delekta, M.M. Laurila, M. Mäntysalo, J. Li, Nano-Micro Lett. 12 (2020) 40.
[212] J.G. Sánchez, V.S. Balderrama, S.I. Garduño, E. Osorio, A. Viterisi, M. Estrada, J. Ferré-Borrull, J. Pallarès, L.F. Marsal, RSC Adv. 8 (2018).
[213] S.H. Eom, H. Park, S.H. Mujawar, S.C. Yoon, S.S. Kim, S.I. Na, S.J. Kang, D. Khim, D.Y. Kim, S.H. Lee, Org. Electron. 11 (2010) 1516–1522.
[214] S. Il Ahn, W.K. Kim, S.H. Ryu, K.J. Kim, S.E. Lee, S.H. Kim, J.C. Park, K.C. Choi, Org. Electron. 13 (2012) 980–984.
[215] M. Rai, L.H. Wong, L. Etgar, J. Phys. Chem. Lett. 11 (2020).
[216] F. Wang, J.H. Gosling, G.F. Trindade, G.A. Rance, O. Makarovsky, N.D. Cottam, Z. Kudrynskyi, A.G. Balanov, M.T. Greenaway, R.D. Wildman, R. Hague, C. Tuck, T.M. Fromhold, L. Turyanska, Adv. Funct. Mater. (2021) 31.
[217] J. Shi, J. Jie, W. Deng, G. Luo, X. Fang, Y. Xiao, Y. Zhang, X. Zhang, X. Zhang, Adv. Mater. 34 (2022), 2200380.
[218] K. Liang, R. Wang, B. Huo, H. Ren, D. Li, Y. Wang, Y. Tang, Y. Chen, C. Song, F. Li, B. Ji, H. Wang, B. Zhu, ACS Nano 16 (2022) 8651–8661.
[219] Y.G. Kim, D. Lv, J. Huang, R.N. Bukke, H. Chen, J. Jang, Phys. Status Solidi 217 (2020), 2000314.
[220] K.J. Yoon, J.W. Han, D.I. Moon, M.L. Seol, M. Meyyappan, H.J. Kim, C.S. Hwang, Nanoscale Adv. 1 (2019) 2990–2998.
[221] E. Carlos, J. Deuermeier, R. Branquinho, C. Gaspar, R. Martins, A. Kiazadeh, E. Fortunato, J. Mater. Chem. C 9 (2021) 3911–3918.
[222] H. Hu, A. Scholz, C. Dolle, A. Zintler, A. Quintilla, Y. Liu, Y. Tang, B. Breitung, G. C. Marques, Y.M. Eggeler, Adv. Funct. Mater. (2023), 2302290.
[223] S. Porro, C. Ricciardi, RSC Adv. 5 (2015) 68565–68570.
[224] J.U. Lind, T.A. Busbee, A.D. Valentine, F.S. Pasqualini, H. Yuan, M. Yadid, S. J. Park, A. Kotikian, A.P. Nesmith, P.H. Campbell, J.J. Vlassak, J.A. Lewis, K. K. Parker, Nat. Mater. 16 (2017) 303–308.
[225] L. Zhou, X. Chen, W. Su, Z. Cui, W.Y. Lai, Adv. Mater. Interfaces 9 (2022), 2102548.
[226] T.K. Kang, Coatings 11 (2021) 51.
[227] E. Bihar, S. Wustoni, A.M. Pappa, K.N. Salama, D. Baran, S. Inal, NPJ Flex. Electron. 2 (2018) 1–8.
[228] L. Li, L. Pan, Z. Ma, K. Yan, W. Cheng, Y. Shi, G. Yu, Nano Lett. 18 (2018) 3322–3327.
[229] V. Dua, S.P. Surwade, S. Ammu, S.R. Agnihotra, S. Jain, K.E. Roberts, S. Park, R. S. Ruoff, S.K. Manohar, Angew. Chemie 122 (2010) 2200–2203.
[230] Y. Qin, H.J. Kwon, A. Subrahmanyam, M.M.R. Howlader, P.R. Selvaganapathy, A. Adronov, M.J. Deen, Mater. Lett. 176 (2016) 68–70.
[231] P. Lorwongtragool, E. Sowade, N. Watthanawisuth, R.R. Baumann, T. Kerdcharoen, Sensors (Basel) 14 (2014) 19700–19712.
[232] M.J. Grotevent, C.U. Hail, S. Yakunin, D. Bachmann, M. Calame, D. Poulikakos, M.V. Kovalenko, I. Shorubalko, Adv. Sci. 8 (2021), 2003360.
[233] H.C. Wang, Y. Hong, Z. Chen, C. Lao, Y. Lu, Z. Yang, Y. Zhu, X. Liu, Nanoscale Res. Lett. 15 (2020).
[234] G. Pace, A. Grimoldi, D. Natali, M. Sampietro, J.E. Coughlin, G.C. Bazan, M. Caironi, Adv. Mater. 26 (2014) 6773–6777.
[235] S. Ma, F. Ribeiro, K. Powell, J. Lutian, C. Møller, T. Large, J. Holbery, ACS Appl. Mater. Interfaces 7 (2015) 21628–21633.
[236] G. Barrett, R. Omote, Inf. Disp. 26 (2010) 16–21 (1975).
[237] L.M. Faller, W. Granig, M. Krivec, A. Abram, H. Zangl, J. Micromech. Microeng. 28 (2018), 104002.
[238] L.M. Faller, M. Lenzhofer, C. Hirschl, M. Kraft, H. Zangl, Sensors 19 (2019) 443.
[239] S. Yang, N. Lu, Sensors 13 (2013) 8577–8594.
[240] D. Barmpakos, A. Segkos, C. Tsamis, G. Kaltsas, Proceedings 2 (2018) 977.
[241] M.D. Dankoco, G.Y. Tesfay, E. Benevent, M. Bendahan, Mater. Sci. Eng. B 205 (2016) 1–5.
[242] C. Bali, A. Brandlmaier, A. Ganster, O. Raab, J. Zapf, A. Hübler, Mater. Today Proc. 3 (2016) 739–745.
[243] T. Vuorinen, J. Niittynen, T. Kankkunen, T.M. Kraft, M. Mäntysalo, Sci. Rep. 6 (2016) 35289.

[244] A. Borenstein, O. Hanna, R. Attias, S. Luski, T. Brousse, D. Aurbach, J. Mater. Chem. A 5 (2017) 12653–12672.
[245] G. Li, Z. Meng, J. Qian, C.L. Ho, S.P. Lau, W.Y. Wong, F. Yan, Mater. Today Energy 12 (2019) 155–160.
[246] M. Maximov, D. Kolchanov, Il. Mitrofanov, A. Vinogradov, Y. Koshtyal, A. Rymyantsev, A. Popovich, Proceedings 3 (2018) 7.
[247] C.A. Milroy, S. Jang, T. Fujimori, A. Dodabalapur, A. Manthiram, Small 13 (2017) 1–11.
[248] S. Lawes, Q. Sun, A. Lushington, B. Xiao, Y. Liu, X. Sun, Nano Energy 36 (2017) 313–321.
[249] P.E. Delannoy, B. Riou, T. Brousse, J.Le Bideau, D. Guyomard, B. Lestriez, J. Power Sources 287 (2015) 261–268.
[250] J. Hu, Y. Jiang, S. Cui, Y. Duan, T. Liu, H. Guo, L. Lin, Y. Lin, J. Zheng, K. Amine, F. Pan, Adv. Energy Mater. 6 (2016), 1600856.
[251] F. Zhang, M. Wei, V.V. Viswanathan, B. Swart, Y. Shao, G. Wu, C. Zhou, Nano Energy 40 (2017) 418–431.
[252] C.C. Ho, K. Murata, D.A. Steingart, J.W. Evans, P.K. Wright, J. Micromech. Microeng. 19 (2009), 094013.
[253] P.E. Delannoy, B. Riou, B. Lestriez, D. Guyomard, T. Brousse, J.Le Bideau, J. Power Sources 274 (2015) 1085–1090.
[254] Elephantech Inc, Https://Www.Elephantech.Co.Jp/En/(2021).
[255] PV Nano Cell Ltd, Https://Www.Pvnanocell.Com/(2021).
[256] BotFactory, Https://Www.Botfactory.Co/Page/Botfactory-Sv2-Pcb-Printer (2021).
[257] Nano Dimens. Https://Www.Nano-Di.Com/Ame-Materials (2021).
[258] J.S. Park, H.J. Choi, G.D. Han, J. Koo, E.H. Kang, D.H. Kim, K. Bae, J.H. Shim, J. Power Sources 482 (2021), 229043.
[259] M. Kim, D.H. Kim, G.D. Han, H.J. Choi, H.R. Choi, J.H. Shim, J. Alloys Compd. 843 (2020), 155806.
[260] L. Hakola, A. Parra Puerto, A. Vaari, T. Maaninen, A. Kucernak, S. Viik, M. Smolander, Flex. Print. Electron. 5 (2020), 025002.
[261] E. Sowade, M. Polomoshnov, A. Willert, R.R. Baumann, Adv. Eng. Mater. 21 (2019), 1900568.
[262] K. Kowsari, S. Akbari, D. Wang, N.X. Fang, Q. Ge, 3D Print, Addit. Manuf. 5 (2018) 185–193.
[263] A. Scholz, L. Zimmermann, U. Gengenbach, L. Koker, Z. Chen, H. Hahn, A. Sikora, M.B. Tahoori, J. Aghassi-Hagmann, Nat. Commun. 11 (2020).
[264] Y. Fang, X. Wu, S. Lan, J. Zhong, D. Sun, H. Chen, T. Guo, ACS Appl. Mater. Interfaces 10 (2018) 30587–30595.
[265] J.A. Lim, J.H. Kim, L. Qiu, W.H. Lee, H.S. Lee, D. Kwak, K. Cho, Adv. Funct. Mater. (2010) 20.
[266] M.F. Farooqui, M.A. Karimi, K.N. Salama, A. Shamim, Adv. Mater. Technol. 2 (2017), 1700051.
[267] J. Kwon, Y. Takeda, R. Shiwaku, S. Tokito, K. Cho, S. Jung, Nat. Commun. 10 (2019) 54.
[268] J. Kwon, Y. Takeda, K. Fukuda, K. Cho, S. Tokito, S. Jung, ACS Nano 10 (2016) 10324–10330.
[269] J. Kwon, Y. Takeda, K. Fukuda, K. Cho, S. Tokito, S. Jung, Adv. Electron. Mater. 2 (2016), 1600046.
[270] K. Fukuda, Y. Takeda, Y. Yoshimura, R. Shiwaku, L.T. Tran, T. Sekine, M. Mizukami, D. Kumaki, S. Tokito, Nat. Commun. 5 (2014) 4147.
[271] J. Fang, W. Deng, X. Ma, J. Huang, W. Wu, IEEE Electron Device Lett. 38 (2016) 183–186.
[272] K. Fukuda, T. Someya, Adv. Mater. 29 (2017), 1602736.
[273] W. Tang, Y. Huang, L. Han, R. Liu, Y. Su, X. Guo, F. Yan, J. Mater. Chem. C 7 (2019) 790–808.
[274] H. Cho, Y. Lee, B. Lee, J. Byun, S. Chung, Y. Hong, J. Inf. Disp. (2019) 0316.
[275] T. Zhang, E. Asher, J. Yang, Adv. Mater. Technol. 3 (2018), 1700346.
[276] M. Kang, K.T. Kang, Int. J. Precis. Eng. Manuf. Green Technol. 5 (2018) 421–426.
[277] Constantine A. Balanis, Antenna Theory: Analysis and Design, 4th Edn., John Wiley & Sons, 2016.
[278] A. Alex-Amor, Á. Palomares-Caballero, J. Moreno-Núñez, A. Tamayo-Domínguez, C. García-García, J.M. Fernández-González, Microw. Opt. Technol. Lett. 63 (2021) 1719–1726.
[279] M.A. Monne, P.M. Grubb, H. Stern, H. Subbaraman, R.T. Chen, M.Y. Chen, Micromachines 11 (2020) 1–12.
[280] What Is PolyJet Technol. 3D Printing? | Strat. Https://Www.Stratasys.Com /Polyjet-Technology (2021).
[281] M.F. Farooqui, A. Shamim, IEEE Antennas Wirel. Propag. Lett. 16 (2017) 800–803.
[282] J. Kimionis, M. Isakov, B.S. Koh, A. Georgiadis, M.M. Tentzeris, IEEE Trans. Microw. Theory Tech. 63 (2015) 4521–4532.
[283] T. Tilford, S. Stoyanov, J. Braun, J.C. Janhsen, M.K. Patel, C. Bailey, IEEE Trans. Compon. Packag. Manuf. Technol. 11 (2021) 351–362.